AN INVESTIGATION OF THE CHARACTERISTICS OF VIBRATORY RATE GYROSCOPES

by

R. F. McLEAN, A.R.C.S.T.

Thesis submitted to the University of Edinburgh
for the degree of Master of Science.

OCTOBER 1961

The author wishes to express his appreciation to Professor R. N. Arnold, D.Sc., D.Eng., Ph.D., M.I.Mech.E., M.I.C.E., and Professor L. Maunder, B.Sc., Sc.D., Ph.D., for their guidance and helpful suggestions throughout this work.

SYNOPSIS

This thesis commences with an analysis of the cyclic variation in the bending natural frequency of the tines of the tuning fork as it is orientated in the gravitational field. The analytical solution gives a value which deviates by less than ten per cent from the experimental value obtained by other authors and therefore suggests a possible explanation of this previously unexplained variation.

The torsion gyro, which forms the main part of this text, is an alternative to the tuning fork as a vibratory rate gyroscope. The instrument appears to be a new concept in this field and seems to have advantages over the tuning fork. Its configuration and method of operation are described and some of its main characteristics investigated. These include the analysis of the balanced system and its transient response, the effects of unbalance and the damping characteristics of the system. Design graphs are drawn to enable approximate numerical values to be established and a suggestion is made for a suitable type of instrumentation.

The theoretical results agree closely with those obtained experimentally. It was necessary to operate the instrument with high input rates of turn, but it has been shown that the instrument is capable of detecting reasonably small inputs.

Contents

Contents (Cont'd)

Page No.

CHAPTER I

1.0 Introduction

During the present century the gyroscope has experienced innumerable modifications and improvements which have increased its accuracy, sensitivity and range of application. In the field of navigation, where increasingly severe demands are being made on this instrument, inaccuracies previously tolerated could impose detrimental acceleration forces on the human body while travelling at supersonic speeds. It is apparent that each additional refinement becomes more difficult to produce and the expense of manufacturing high precision gyroscopes increases accordingly. With the growing complexity in producing present day gyroscopes it would seem that a basic change is required from the conventional spinning wheel type of instrument developed over one hundred years ago by Foucault. The vibratory rate gyroscope emerged as a result of these considerations. A parallel to this can be seen in prime movers where steam power was becoming increasingly impracticable in the form of the reciprocating engine but was completely revolutionized with the advent of the steam turbine.

Numerous authors have contributed papers on the use of the tuning fork as a rate of turn indicator, amongst the first being Pringle (Reference 9) in which he describes the flight controls of the Diptera insect,

one of which is the common fly. This insect has protruding from its thorax two large club shaped halteres which oscillate through a large amplitude about the vertical plane. By inter-muscular action the insect, as it turns about the vertical axis, detects Coriolis forces incurred in the vibrating halteres. This biological action is similar to the action of the tuning fork when used as a vibratory rate gyroscope. In the tuning fork the tines oscillate through small amplitudes giving a radial velocity to the mass of the tines which, together with a rotation of the stem, induces oscillating Coriolis forces to be superimposed on the stem. This can also be visualised from the principle of the conservation of angular momentum applied to the complete tuning fork about its stem. As the inertia of the tine increases on its outward swing the velocity of rotation of the stem must decrease to compensate for this and maintain constant angular momentum within the system. With a corresponding increase in rotational velocity as the tines swing inwards, a periodic oscillatory motion is superimposed on the applied rate of turn. The amplitude and phase of this oscillatory output is a measure of the velocity and direction of the applied rate of turn.

A considerable amount of research has been

carried out to establish the tuning fork as an accurate rate of turn meter. It can be seen from references (10) and (11) that the Sperry Gyroscope Company anticipated a great future for this instrument. However, after a considerable amount of research, they appear to have abandoned the project. One of their major difficulties was the inability to eliminate output signals arising from small inaccuracies in the manufacture of the tines. Another significant source of error experienced by other authors, is the sensitivity of the tuning fork to its position in the gravitational field. This is more fully discussed in the next chapter.

The main part of this thesis is concerned with the investigation of a new type of vibratory rate gyro. This instrument is a departure from the tuning fork and appeared at the outset to be a new concept in this field. The configuration of the instrument, as can be seen from figure (1), is similar to the more conventional gyroscope except that the shafts are rigidly fixed and the rotor oscillates rather than rotates. The fundamental difference between this torsion gyro instrument and the tuning fork is in the primary system. In the tuning fork this consists of a lateral vibration of the tines instead of the torsional oscillation experienced in the 'rotor' of the torsion gyro. The secondary, or output systems of both are

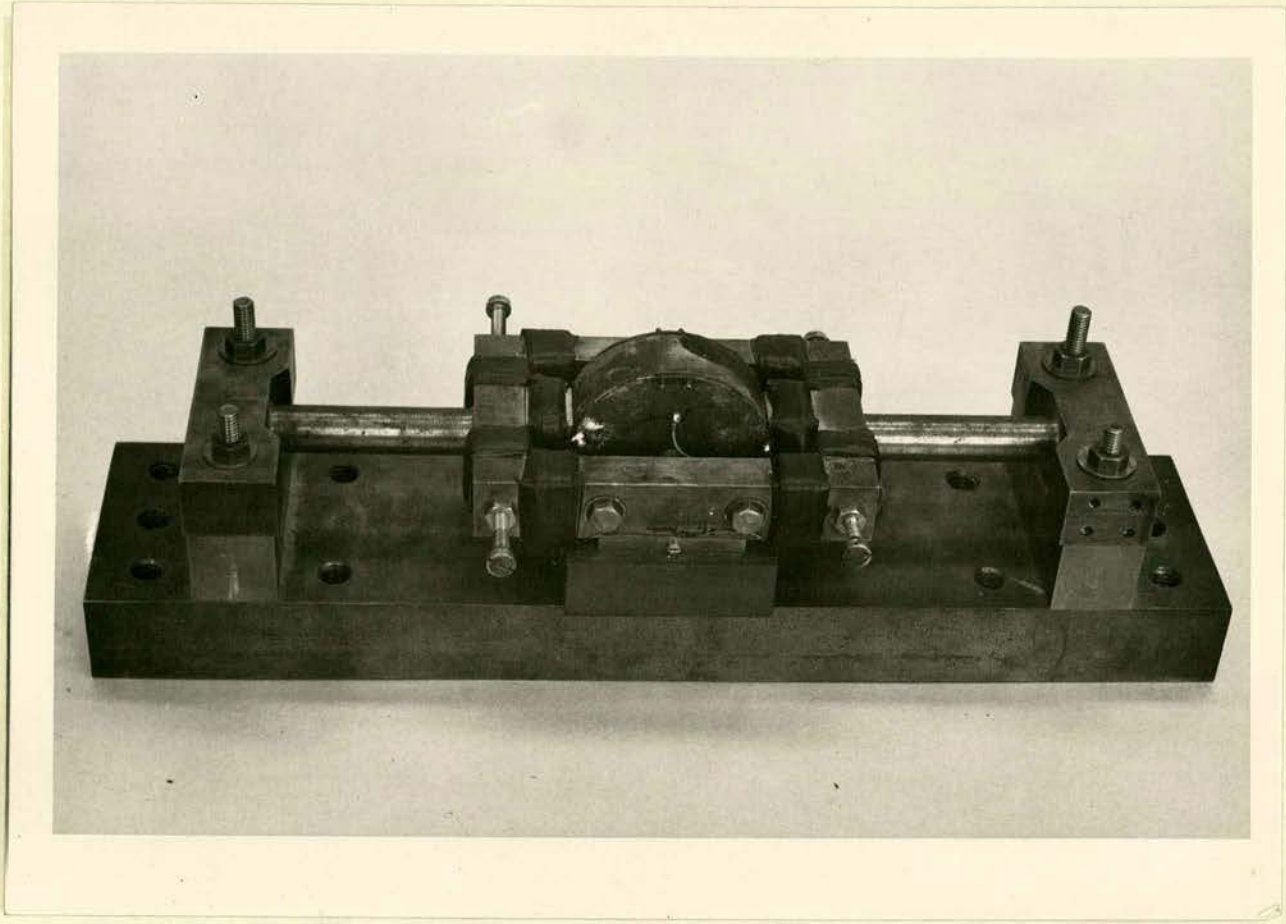

FIG. 1. ASSEMPLED INSTRUMENT WITH CAPACITANCE PICK-UP

similar in that they are in torsional oscillation about their output shafts. However, in the torsion gyro this output shaft is not the same as the applied rate of turn axis as is the case in the tuning fork.

Vibratory rate gyros, because of their unit construction, are more robust than the conventional form of gyroscope. The principal advantage is the absence of bearings which eliminates friction and wear, thereby reducing replacement and maintenance costs. The output being oscillatory has advantages, as far as measurement is concerned, over the constant form of output obtained in the more conventional type of gyroscope.

CHAPTER 2

2.0 Tuning Fork

In the tuning fork, when used as a vibratory rate gyroscope, the tines are generally excited at their natural frequency of bending by electromagnets. The energy input has therefore to compensate only for the loss due to damping within the system. When a rotation is applied to the stem of the instrument, the combination of this rotation and the radial velocity of the tines produces Coriolis forces on the tines, a torque thereby being applied to the torsional stem. To obtain maximum response, the natural frequency of the torsional system is made equal to the bending natural frequency of the tines.

Experimental work carried out by previous authors detected a cyclic variation in the bending natural frequency of the tines as the tuning fork was orientated in the gravitational field. Due to this variation, the tuning of the bending frequency to the torsional natural frequency of the stem cannot be established and the response is correspondingly reduced. This effect was considered by those authors to be the greatest source of uncertainty in the instrument. An analysis of a possible source of this variation is therefore discussed in detail in the following paragraphs.

2.1 Gravitational Effects

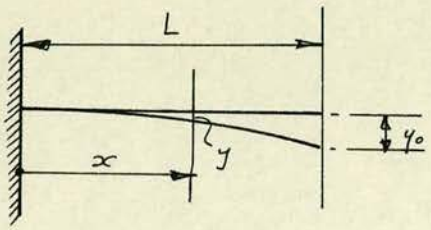

FIG. 2.

By considering the tines as cantilevers fixed rigidly to the heel of the fork (Fig.2), the bending natural frequency of the tines can be evaluated by the Rayleigh method. As the basis of this calculation the shape of the tine during vibration must be assumed; in this case a quarter cosine wave has the requisite properties, i.e. horizontal at $x = 0$ and having no curvature or bending moment at $x = L$.

$$\therefore\ y = y_o\left(1 - \cos\frac{\pi x}{2L}\right) \qquad \text{——————(1)}$$

With this assumption the maximum potential and kinetic energies are calculated and equated to give the frequency of vibration. The maximum potential energy of bending occurs when the tine reaches its maximum deflected form and can be evaluated from the characteristic equation:-

$$\text{Potential Energy} = V = \frac{EI}{2}\int_0^L \left(\frac{d^2y}{dx^2}\right)^2 dx \qquad \text{——————(2)}$$

where E and I are respectively Young's Modulus of Elasticity and Moment of Inertia in bending of the tine.

By the substitution of equation (1) into equation (2) the maximum potential energy is found to be:-

$$V = \frac{\pi^4}{64} \frac{EI}{L^3} y_o^2 \qquad \text{——————————} (3)$$

The maximum kinetic energy occurs when the tine is in the mid position and can be found from:-

$$\text{Maximum Kinetic Energy} = T = \frac{\omega p^2}{2g} \int_0^L y^2 dx \qquad \text{——} (4)$$

where ω is the weight per unit length of the tine material and p is the frequency of vibration.

Substituting equation (1) into equation (4) gives the maximum kinetic energy as:-

$$T = \frac{\omega}{g} p^2 y_o^2 L \left[\frac{3}{4} - \frac{2}{\pi}\right] \qquad \text{——————————} (5)$$

By equating equations (3) and (5) an approximate expression for the frequency of vibration can be found for the tine considered as a cantilever vibrating under the action of its own mass per unit length.

As a part of the electrostatic drive system, the instrument under consideration had masses attached to the end of the tines. The potential energy of the tine is not affected by the addition of this mass but since the amplitude of the end of the tine is y_o the kinetic energy is increased by $\frac{1}{2} \frac{W}{g} p^2 y_o^2$ where W is the weight of the end mass.

The total kinetic energy is therefore:-

$$T = \frac{p^2 y_0^2}{2g}\left[W + \omega L\left(\frac{3}{2} - \frac{4}{\pi}\right)\right] \qquad (6)$$

The frequency can then be found by equating (3) and (6)

$$\text{i.e. } p^2 = \frac{3{\cdot}03\,EIg}{L^3\left[W + 0{\cdot}23\,\omega L\right]} \qquad (7)$$

This expression holds good for the condition when the tines are lying in the horizontal plane, i.e. when $\theta = 0$. As the fork is orientated in the gravitational field, the mass of the tine material and the end loads cause axial forces to be impressed on the tines in addition to those previously considered. The potential energy of the tines is therefore increased or decreased depending upon whether the axial forces are tensile $(\pi < \theta < 2\pi)$ or compressive $(0 < \theta < \pi)$ When θ equals zero or π corresponding to the tine lying in the horizontal position, the axial forces are zero and equation (7) can be used to obtain the bending natural frequency.

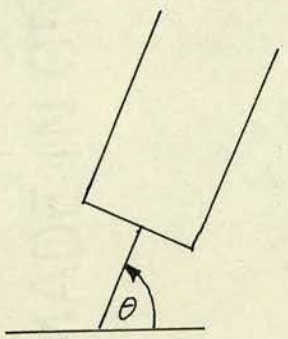

FIG. 3.

Timoshenko (Reference 1) shows that the changes in potential energy due to the axial load effect of the end mass and tine material are respectively:-

$$\Delta V_1 = \frac{S}{2}\int_0^L \left(\frac{dy}{dx}\right)^2 dx \qquad (8)$$

and $$\Delta V_2 = \frac{\phi}{2}\int_0^L \left(\frac{dy}{dx}\right)^2 (L-x)\,dx \qquad \text{——————(9)}$$

where, from figure 4 it can be seen that:-

$$\left.\begin{aligned} S &= -W\sin\theta \\ \phi &= -\omega\sin\theta \end{aligned}\right\} \text{——(10)}$$

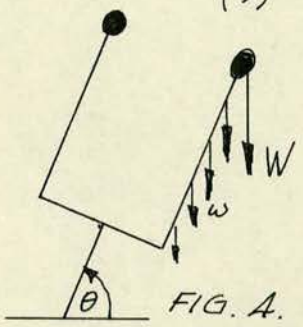

FIG. 4.

By substituting the derivative of equation (1) in equations (8) and (9) and then integrating between the limits 0 and L the change in potential energy becomes:-

$$\Delta V_1 = -\frac{W y_o^2 \pi^2}{16L}\sin\theta \qquad \text{——————(11)}$$

and $$\Delta V_2 = -\frac{\omega y_o^2}{32}(\pi^2 - 4)\sin\theta \qquad \text{——————(12)}$$

The total potential energy of the tine, therefore, from equations (3), (11) and (12) becomes:-

$$V = \frac{\pi^4 EI}{64 L^3} y_o^2 - \left[\frac{W y_o^2 \pi^2}{16L} + \frac{\omega y_o^2}{32}(\pi^2 - 4)\right]\sin\theta \text{——(13)}$$

Equations (6) and (13) are then equated to give the frequency equation:-

$$p^2 = \frac{\pi^2 2g\left[\frac{\pi^2 EI}{4L^2} - \left\{W + \frac{\omega L}{2}\left(1 - \frac{4}{\pi^2}\right)\right\}\sin\theta\right]}{16L\left[W + 0{\cdot}23\,\omega L\right]} \text{——(14)}$$

The experimental instrument, in which this variation in tine frequency was observed, had the following approximate characteristics:-

$$E = 2 \times 10^{12} \text{ dynes/cm.}^2$$

$$I = 1/12 \times 2 \times 0{\cdot}4^3 \text{ cm.}^4$$

$L = 5{\cdot}7$ cm.

$W = 34{\cdot}65$ gms.

$\omega = 6.16$ gm/cm.

By substituting the above numerical values in equation (14) the bending natural frequency can be obtained.

$$\therefore p^2 = 8{\cdot}2 \times 10^{-6}\left[1 - 27{\cdot}5 \times 10^{-6} \sin\theta\right] \qquad (15)$$

$$\therefore p = 2860\left[1 - 27{\cdot}5 \times 10^{-6} \sin\theta\right]^{\frac{1}{2}} \qquad (16)$$

The maximum effect due to gravity occurs when the fork is in either of its vertical positions, i.e. when $\theta = \frac{\pi}{2} \& \frac{3\pi}{2}$ and $\sin\theta = \pm 1$. By expanding equation (16) from the Binomial Theorem, the frequency (p) can be expressed as:-

$$p = 2860\left[1 \pm 13{\cdot}75 \times 10^{-6} \sin\theta\right] \qquad (17)$$

Equation (17) shows that there is approximately $\pm 13{\cdot}75$ parts per million sinusoidal variation in the time bending frequency due to the orientation of the tuning fork in the gravitational field. The instrument , in which previous authors detected this variation, gave an experimental value of ± 15 parts per million. The approximate nature of the dimensions given does not allow correlation of the experimental frequency of 394 c.p.s. and the calculated result of 455 c.p.s. but the nearness of the experimental and theoretical frequency change shows that the above analysis indicates a possible explanation of this troublesome phenomenon.

CHAPTER 3

3.0 Torsion Gyro

The torsion gyro, which forms the main part of this text, is in its early development and only a few of the main characteristics could be investigated during the current research period. As this is an entirely new type of instrument, some of these characteristics must take the form of a design study rather than a more full investigation of its possible applications. The configuration of the instrument, as discussed earlier and illustrated in figure 1, is similar to the more conventional type of gyroscope with the exception that there are no bearings and the 'rotor', instead of spinning at a high velocity, oscillates torsionally about the rotor shafts.

One of the principal difficulties experienced with the tuning fork is the accurate manufacture of the tines. This, to a great extent, is overcome in the torsion gyro as the 'rotor', being a solid of revolution, can be more accurately manufactured than the tines of the tuning fork. Also a balancing out procedure, as illustrated in Chapter 4.5 can be carried out relatively easily on the 'rotor' of this instrument. The 'rotor' also gives a well defined plane of vibration as compared to the plane of vibration of the tines of the tuning fork, which depend upon the relative stiffness of the tine in its plane of vibration and the

plane at right angles to it. The gravitational effects occurring in the tuning fork and discussed in the previous chapter are not incurred in the torsion gyro.

The method of exciting the 'rotor' of the torsion gyro is one of the major disadvantages of this type of instrument and compares unfavourably with the electromagnetic or electrostatic drive employed to oscillate the tines of the tuning fork.

The remainder of this text is concerned with the analysis of some of the aspects of the torsion gyro.

3.1 Analysis of the Balanced System

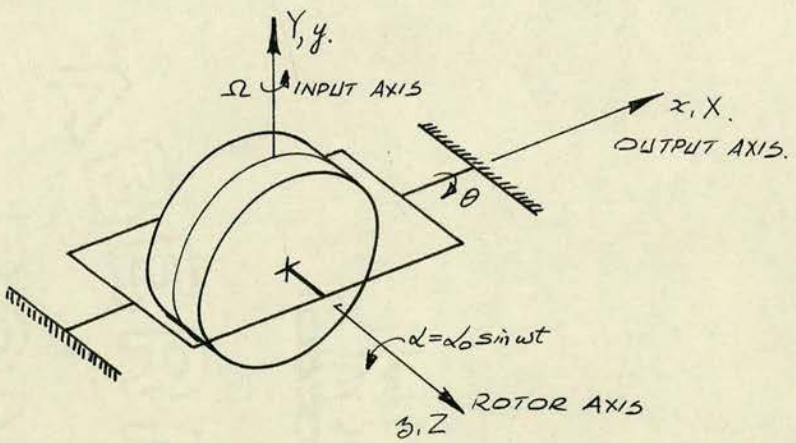

FIG. 5.

Figures 1 and 5 illustrate the arrangement of the torsion gyro. The rotor is free to oscillate about its axis oz while the gimbal in which the rotor shafts are mounted can oscillate about the output axis ox. The output shafts are mounted on the frame of the instrument, about which, the input signal is applied.

The rotor is vibrated by inducing a magnetic flux to flow between two pole pieces mounted on the gimbal, at the rotor periphery (Fig.1). Near the periphery of the rotor, conductors are inserted parallel to the axis of the rotor shafts. An alternating current is applied to those conductors to give the torsional oscillation of the rotor.

When a rate of turn signal is applied to the base of the instrument, the combination of this input and the sinusoidal momentum induces Coriolis forces on the rotor, acting at right angles to the rotor and input axes. These Coriolis forces therefore develop a torque which varies at the frequency of the rotor velocity, thereby giving, via the output shafts, a torsional output to the gimbal system.

To obtain the maximum response possible from the system, the frequency of the rotor oscillations is made equal to the undamped natural frequency of both the rotor and gimbal systems oscillating about their torsional shafts.

In this idealized system, it is assumed that the instrument is symmetrical about the rotor and output gimbal axes, the two axes of symmetry intersecting at the centre of the rotor. The two systems oscillate entirely about their respective axes. It is further assumed that the bending

frequencies of the rotor mounted in the gimbal, and the gimbal mounted within the frame, are not within the range of the operating torsional frequency.

Figure 5 shows a diagrammatic arrangement of the torsion gyro. The orthogonal axes $OXYZ$ are principal axes considered attached to the base of the instrument and $oxyz$ are also principal axes attached to the gimbal. $OXYZ$ coincides with $oxyz$ when θ the torsional output of the gimbal is zero. Consider the rotor (α) and output (θ) oscillations to be small and $\bar{I},\bar{J},\bar{K}$, and $\bar{\imath},\bar{\jmath}\,\bar{k}$ to be unit vectors along the respective orthogonal axes $OXYZ$ and $oxyz$.

With an input velocity Ω applied to the instrument it can be seen, by resolving angular velocities about their orthogonal axes, that:-

$$\left.\begin{aligned}&\text{Instrument angular velocity } \Omega=\Omega_1\bar{I}+\Omega_2\bar{J}+\Omega_3\bar{K}\\&\text{Gimbal angular velocity } \bar{\omega}=(\Omega_1+\dot{\theta})\bar{\imath}+(\Omega_2+\Omega_3\theta)\bar{\jmath}+(\Omega_3-\Omega_2\theta)\bar{k}\\&\text{Rotor angular velocity } =\bar{\omega}+\dot{\alpha}\bar{k}\end{aligned}\right\}(18)$$

A, B and C refer to the principal moments of inertia of the system about the orthogonal axes which, when included with the subscripts 'i' and 'o', refer only to the inner rotor and outer gimbal system respectively. The angular momentum of the rotor and gimbal systems about the $oxyz$ axes can be expressed as:-

$$\bar{h}=A(\Omega_1+\dot{\theta})\bar{\imath}+B(\Omega_2+\Omega_3\theta)\bar{\jmath}+\left[C(\Omega_3-\Omega_2\theta)+C_1\dot{\alpha}\right]\bar{k} \qquad (19)$$

From the angular momentum equation the torque about the x-axis can be expressed in terms of the angular momentum and angular velocities of the rotating axes. This torque can also be equated as the sum of the damping and spring torques provided that the inertia of the output shafts is small compared to the inertia of the gimbal.

$$\text{a}\,T_x = \dot{h}_x - h_y\omega_3 + h_3\omega_y = -C_x\dot{\theta} - k_x\theta \qquad \text{——————} (20)$$

h_x, h_y and h_3 are the components of angular momentum, expressed in equation (19), about the x, y and z axis, ω_y and ω_3 are the components of the gimbal angular velocity, expressed in equation (18), C_x and k_x are the viscous damping and stiffness co-efficients of the gimbal system about the output x-axis. Equation (20) can therefore be expressed as:-

$$\left.\begin{aligned} T_x = {} & A(\dot{\Omega}_1 + \ddot{\theta}) - B(\Omega_2 + \Omega_3\theta)(\Omega_3 - \Omega_2\theta) \\ & + [C(\Omega_3 - \Omega_2\theta) + C_1\dot{\alpha}](\Omega_2 + \Omega_3\theta) = -C_x\dot{\theta} - k_x\theta \end{aligned}\right\} (21)$$

On re-arrangement equation (21) becomes:-

$$A\ddot{\theta} + C_x\dot{\theta} + [k_x + (B-C)(\Omega_2^2 - \Omega_3^2) + C_1\dot{\alpha}\Omega_3]\theta + (B-C)(\Omega_2\Omega_3\theta^2)$$
$$-(B-C)(\Omega_2\Omega_3) + A\dot{\Omega}_1 + C_1\dot{\alpha}\Omega_2 = 0 \qquad \text{——————} (22)$$

This equation is non-linear and has therefore no formal solution. With the range of parameters used for this instrument the terms $(B-C)(\Omega_2^2 - \Omega_3^2)\theta$ and $C_1\dot{\alpha}\Omega_3\theta$ are very much smaller than the shaft stiffness torque $k_x\theta$ and can therefore be neglected from the equation. Since the output θ is small the

equation can be linearized by neglecting the $(B-C)(\Omega_2\Omega_3\theta^2)$ as this is a second order quantity in θ .

Equation (22) can therefore be expressed as the more general linear equation, having several forcing functions.

$$A\ddot{\theta} + C_x\dot{\theta} + k_x\theta = (B-C)\Omega_2\Omega_3 - A\dot{\Omega}_1 - C_1\dot{\alpha}\Omega_2 \qquad (23)$$

This equation shows that the instrument is sensitive to input rates of turn applied about rotor and output axis as well as the rate of turn axis Y . However, with a constant rate of turn signal applied to the instrument, the forcing function $A\dot{\Omega}_1$ will be zero and the forcing function $(B-C)\Omega_2\Omega_3$ will give a solution of constant output. With a pick-up sensitive only to an oscillatory motion this output can be neglected leaving only the output from the forcing function which is proportional to the oscillatory input.

Equation (23) can, therefore, for this constant input rate of turn, be expressed as

$$A\ddot{\theta} + C_x\dot{\theta} + k_x\theta = -C_1\dot{\alpha}\Omega_2 \qquad (24)$$

With $\alpha = \alpha_0 \sin\omega t$ this equation becomes the familiar second order forced vibration equation with a solution containing the complementary function for the free vibration and the particular integral for the forced vibration. The free vibration solution rapidly approaches zero and the steady state solution remains, giving:-

$$\theta = -\frac{\alpha_0\omega C_1\Omega_2\cos(\omega t - \phi)}{A\sqrt{(\omega_n^2-\omega^2)^2 + (\frac{C_x}{A}\omega)^2}} \qquad (25)$$

ω_n represents the undamped natural frequency equal to $\sqrt{k_x/A}$ and ω is the forcing frequency of the system. The phase angle ϕ equal to $\tan^{-1}\frac{\omega C_x}{A(\omega_n^2-\omega^2)}$ determines the phase of the output relative to the rotor amplitude $\alpha=\alpha_0 \sin\omega t$. Equation (25) can be stated in its non dimensional form by substituting f the frequency ratio equal to ω/ω_n and d the damping ratio equal to C_x/C_c , where C_c is the critical damping coefficient equal to $2A\omega_n$.

$$\theta = -\frac{\alpha_0 f C_1 \Omega_z \cos(\omega t-\phi)}{A\omega_n\sqrt{(1-f^2)^2+(2fd)^2}} \qquad (26)$$

The maximum response of the system occurs when the forcing frequency equals the undamped natural frequency, i.e. the frequency ratio is equal to unity, this condition being referred to as the tuned resonant condition.

This gives the solution:-

$$\theta = \frac{\alpha_0 C_1 \Omega_z \sin\omega t}{2A\omega_n d} \qquad (27)$$

This solution shows that the response of the system is proportional to the rotor amplitude α_0 , the applied rate of turn Ω_z and the inertia ratio C_1/A and inversely proportional to the damping coefficient d and the torsional frequency ω_n . The phase of the output at this tuned resonant condition, is the same as that of the sinusoidal rotor oscillation for a positive rate of turn, and 180° out of phase for negative rates

of turn. The direction of rotation as well as the magnitude of the input rate of turn being determined by this equation. With a constant rate of turn it can be seen that the instrument is sensitive only to rates of turn applied about the input axis.

3.2 Response to Sinusoidal Inputs

The response to a step function and a sinusoidal input, form two of the basic tests carried out on a rate of turn gyroscope which is to be included as part of a servo-system. The former is discussed in paragraph 3.3, whilst the latter is analysed in this present section.

Assume a sinusoidal input $\Omega = \Omega' \sin qt$ is applied to the system. Where Ω' is the maximum velocity and q is the frequency of the applied input, this input can be resolved about the orthogonal axes. By substitution in equation (23) of the previous paragraph, equation (28) can be obtained.

$$A\ddot{\theta} + C_x\dot{\theta} + k_x\theta = (B-C)\Omega_2'\Omega_3' \sin^2 qt - Aq\Omega_1' \cos qt - C_1\alpha_0\omega\Omega_2' \sin \omega t \sin qt \quad \text{---(28)}$$

Which, on rearrangement becomes:-

$$\ddot{\theta} + \frac{C_x}{A}\dot{\theta} + \omega_n^2\theta = F_1 \sin \omega t \sin qt + F_2 \cos qt + F_3 \sin^2 qt \quad \text{---(29)}$$

where $F_1 = -\frac{C_1}{A}\alpha_0\omega\Omega_2'$

$F_2 = -\Omega_1' q$

$F_3 = \frac{(B-C)}{A}\Omega_2'\Omega_3'$

Expanding equation (29) to obtain:-

$$\ddot{\theta} + \frac{C_x}{A}\dot{\theta} + \omega_n^2\theta = F_1/2\left[\cos(\omega-\varrho)t - \cos(\omega+\varrho)t\right]$$

$$+ F_2\cos\varrho t + F_3/2\left[1 - \cos 2\varrho t\right] \qquad \text{——————} (30)$$

As equation (30) is a linear equation with constant coefficients, the forcing terms which are constant can be eliminated by pick-ups recording only sinusoidal outputs.

The solution to equation (30) can be found by summing the individual solutions obtained by using each of the forcing terms independently. The steady state solution, neglecting constant forcing terms, therefore becomes:-

$$\theta = \frac{F_1\cos\left[(\omega-\varrho)t - \psi_1\right]}{2\sqrt{\left[\omega_n^2-(\omega-\varrho)^2\right]^2+\left[\frac{C_x}{A}(\omega-\varrho)\right]^2}} - \frac{F_1\cos\left[(\omega+\varrho)t - \psi_2\right]}{2\sqrt{\left[\omega_n^2-(\omega+\varrho)^2\right]^2+\left[\frac{C_x}{A}(\omega+\varrho)\right]^2}}$$

$$+ \frac{F_2\cos(\varrho t - \psi_3)}{2\sqrt{(\omega_n^2-\varrho^2)^2+\left(\frac{C_x}{A}\varrho\right)^2}} - \frac{F_3\cos(2\varrho t - \psi_4)}{2\sqrt{\left[\omega_n^2-4\varrho^2\right]^2+\left[2\frac{C_x}{A}\varrho\right]^2}} \qquad \text{——————} (31)$$

where the phase angles

$$\psi_1 = \tan^{-1}\frac{\frac{C_x}{A}(\omega-\varrho)}{\omega_n^2-(\omega-\varrho)^2}$$

$$\psi_2 = \tan^{-1}\frac{\frac{C_x}{A}(\omega+\varrho)}{\omega_n^2-(\omega+\varrho)^2}$$

$$\psi_3 = \tan^{-1}\frac{\frac{C_x}{A}\varrho}{\omega_n^2-\varrho^2}$$

$$\psi_4 = \tan^{-1}\frac{2\frac{C_x}{A}\varrho}{\omega_n^2-4\varrho^2}$$

Consider the two limiting cases:-

(i) When the input frequency ϱ is equal to the rotor forcing frequency ω.

(ii) When the input frequency is very much less than the rotor forcing frequency.

The rotor frequency is itself equal to the undamped natural frequency ω_n . The second case is more general for a conventional servo-system.

(i) With $q=\omega$ the solution to equation (31) becomes:-

$$\left.\begin{aligned}\theta = &+ \frac{F_1 \cos\psi_1}{2q^2} - \frac{F_1 \cos(2qt-\psi_2)}{2\sqrt{(-3q^2)^2+4q^2(\frac{C_x}{A})^2}} \\ &+ \frac{F_2 \cos(qt-\psi_3)}{2\frac{C_x}{A}q} - \frac{F_3 \cos(2qt-\psi_4)}{2\sqrt{(-3q^2)^2+4q^2(\frac{C_x}{A})^2}}\end{aligned}\right\} (32)$$

By neglecting constant output terms and substituting the non dimensional damping coefficient $d=\frac{C_x}{2A\omega_n}$ it can be seen that for $d\ll 1$, $(3q^2)^2$ is very much greater than $4q^2(\frac{C_x}{A})^2$ The latter term can therefore be neglected in the denominator of equation (32) to give an output of the form:-

$$\theta = \frac{F_1}{6q^2}\cos(2qt-\psi_2)+\frac{F_2}{4q^2d^2}\cos(qt-\psi_3)+\frac{F_3}{6q^2}\cos(2qt-\psi_4) \quad \text{——(33)}$$

Substituting for ψ_2, ψ_3 and ψ_4 gives:-

$$\theta = \left[-\frac{C_1\alpha_0\Omega_2'}{6Aq}+\frac{(B-C)\Omega_2'\Omega_3'}{6Aq^2}\right]\cos(2qt+\tfrac{4}{3}d) + \frac{\Omega_1}{4qd}\sin qt \quad \text{——————(34)}$$

With the rate of turn considered to be applied predominately about the input axis, i.e. $\Omega_2' > \Omega_1'$ and Ω_3' equation (34) reduces to:-

$$\theta = -\frac{C_1\alpha_0\Omega_2'}{6Aq}\cos(2qt+\tfrac{4}{3}d) \quad \text{——————(35)}$$

Equation (35) shows that a sinusoidal input applied to the instrument gives an output proportional to,

but at twice the frequency of, the input signal. The response, as can be seen from the comparison of equations (27) and (35), is very much less than that obtained with the constant input discussed in the previous chapter. Equation (27) contains in the denominator the non-dimensional damping factor d which, being very much smaller than unity, provides a higher response from the constant input than from the sinusoidal input.

(ii) With $\omega \gg \varrho$ the steady state solution of equation (31) then becomes :-

$$\left.\begin{aligned} \theta = & \frac{F_1 \cos[(\omega-\varrho)t - \psi_1]}{4\omega\sqrt{\varrho^2 + \omega_n^2 d^2}} - \frac{F_1 \cos[(\omega+\varrho)t - \psi_2]}{4\omega\sqrt{(-\varrho)^2 + \omega_n^2 d^2}} \\ & + \frac{F_2 \cos(\varrho t - \psi_3)}{2\omega_n\sqrt{\omega_n^2 + 4\varrho^2 d^2}} - \frac{F_3 \cos(2\varrho t - \psi_4)}{2\omega_n\sqrt{\omega_n^2 + 16\varrho^2 d^2}} \end{aligned}\right\} \quad (36)$$

where the phase angles $\psi_1 = -\psi_2 = \frac{\omega_n}{\varrho} d$ and $\psi_3 = \frac{2\varrho d}{\omega_n} = \frac{\psi_4}{2}$

With the range of parameters encountered in the torsion gyro it can be reasonably assumed that, with $\omega > \varrho$ and $d \ll 1$, the phase angles ψ_3 and ψ_4 are each equal to zero and ω_n^2 will be far greater than $16\varrho^2 d^2$. By combining the outputs proportional to F_1 and substituting values for F and the phase angle ψ equation (36) can be reduced to,

$$\theta = -\frac{C_1 \alpha_0 \Omega_2' \sin\omega t \sin(\varrho t + \frac{\omega_n}{\varrho} d)}{2A\sqrt{\varrho^2 + \omega^2 d^2}} - \frac{\Omega_1' \varrho}{2\omega_n^2} \cos\varrho t - \frac{(B-C)\Omega_2'\Omega_3'}{2A\omega_n^2} \cos 2\varrho t \qquad (37)$$

As in the previous case, it is assumed that the input is applied predominately about the Y-axis, therefore, the term $\frac{(B-C)\Omega_2'\Omega_3'}{2A\omega_n^2}\cos 2\varrho t$ can be neglected. The second term $\frac{\Omega_1'\varrho}{2\omega_n^2}\cos\varrho t$ may give an appreciable output, depending upon the amplitude of the input angular velocity component acting along the output axis. However, this may also be neglected provided that Ω_1' is equal to zero.

The output proportional to the component of the rate of turn signal acting about the input axis constitutes a response at the forcing frequency which, as shown in figure 6, is in itself modulated at the input frequency ϱ.

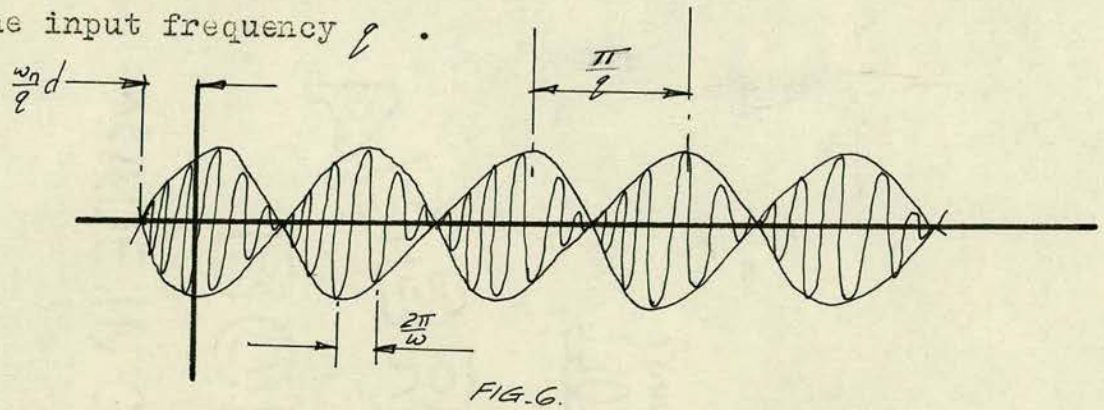

FIG.6.

The peak value of the output is proportional to the maximum value of the sinusoidal input and compares with the output obtained from a constant input previously discussed in paragraph 3.1. The ratio of peak output from a sinusoidal and constant input is $\frac{\varrho^2+\omega^2d^2}{\omega^2d^2}$. This ratio is equal to unity when ϱ is zero as the sinusoidal input is then reduced to a constant input.

3.3 Effect of Transient Response

The effect of the transient response is investigated here by considering the characteristics of the system when the input is changed, by a step function, from a constant applied rate of turn Ω to some new value Ω'.

Until the steady state solution corresponding to the input Ω' is reached, the output will not be representative of the applied rate of turn. The instrument must therefore be considered inoperative during this transient zone. The inoperative time is calculated by matching the steady state solution obtained with the initial rate of turn Ω applied, and the complete solution which includes the transient as well as the steady state solution for the final rate of turn Ω'.

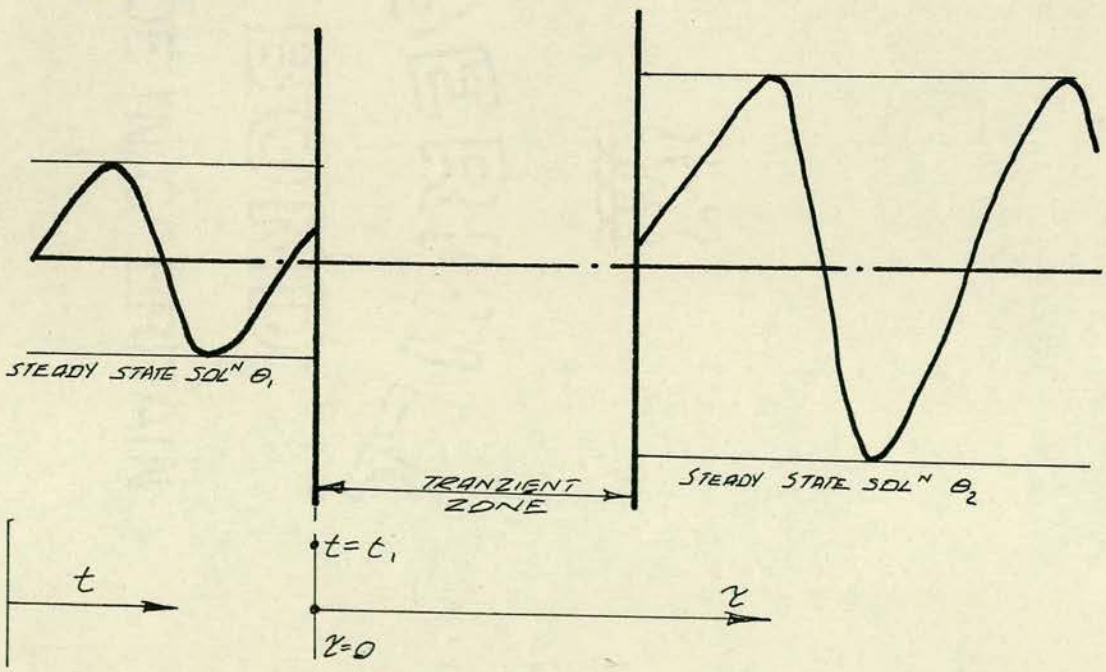

FIG. 7.

Figure 7 shows θ_1 and θ_2 as the steady state solutions from equation (25) corresponding to the applied rates of turn Ω and Ω'. At time $t=t_1$, the step input is applied to give the equivalent output from the new rate of turn Ω', the time thereafter being considered from $\tau = 0$. This output is obtained by summing both the complementary function and the particular integral of the differential equation (24).

i.e. $$\theta_2 = e^{-\Delta\tau}\left[X\cos p\tau + Y\sin p\tau\right] + \frac{C\Omega'\omega\alpha_0\cos(\omega\tau-\phi)}{A\sqrt{(\omega_n^2-\omega^2)^2+(\frac{C_x}{A}\omega)^2}} \qquad (38)$$

X and Y are constants to be determined from initial conditions.

$\omega_n = \sqrt{k_x/A}$ = undamped natural frequency

$\Delta = \frac{C_x}{2A} = \omega_n d$

$p = \sqrt{\omega_n^2 - \Delta^2}$ = damped natural frequency.

The steady state solution corresponding to the rate of turn Ω is, from equation (25), equal to:-

$$\theta = -\frac{\alpha_0\omega C_1\Omega_2\cos(\omega t-\phi)}{A\sqrt{(\omega_n^2-\omega^2)^2+(\frac{C_x}{A}\omega)^2}} \qquad (39)$$

As discussed previously, to obtain maximum response, the system is operated at its tuned resonant condition, i.e. $\omega=\omega_n$. Equations (38) and (39) therefore reduce to:-

$$\theta_2 = e^{-\Delta\tau}\left[X\cos p\tau + Y\sin p\tau\right] + T_2\sin\omega_n\tau \qquad (40)$$

and $\theta_1 = T_1\sin\omega_n t$

where $T_1 = \frac{C_1\Omega\alpha_0}{C_x}$ and $T_2 = \frac{C_1\Omega'\alpha_0}{C_x}$

At the commencement of the step input, i.e. when $t = t_1$ for the initial solution and $\tau = 0$ for the final solution, the velocities and displacements of the system must be equal. Equations (40) and (41) and their derivatives can therefore be equated to give an explicit solution to equation (40).

With $\theta_1 = \theta_2$

$$T_1 \sin \omega_n t_1 = X \qquad \text{——————(42)}$$

and with $\dot{\theta}_1 = \dot{\theta}_2$

$$T_1 \omega_n \cos \omega_n t_1 = -\Delta X + Y/p + T_2 \omega_n \qquad \text{——————(43)}$$

Equation (42) is substituted into equation (43) to obtain Y.

$$\text{i.e. } Y = \frac{T_1 \omega_n \cos \omega_n t_1 + T_1 \Delta \sin \omega_n t_1 - T_2 \omega_n}{p} \qquad \text{——————(44)}$$

Giving as a solution to equation (40).

$$\theta_2 = e^{-\Delta\tau}\left[T_1 \sin \omega_n t_1 \cos p\tau + \left(T_1 \frac{\omega_n}{p} \cos \omega_n t_1 + T_1 \frac{\Delta}{p} \sin \omega_n t_1 - T_2 \frac{\omega_n}{p}\right) \sin p\tau\right]$$

$$+ T_2 \sin \omega_n \tau \qquad \text{——————(45)}$$

By selecting the time $t = t_1$ to correspond to the time when $\sin \omega_n t_1 = 0$ and $\cos \omega_n t_1 = +1$ a simpler solution is obtained.

$$\theta_2 = e^{-\Delta\tau}\left[\frac{\omega_n}{p}(T_1 - T_2) \sin p\tau\right] + T_2 \sin \omega_n \tau \qquad \text{——————(46)}$$

Theoretically the time for the transient response to become zero is infinite but the effect of the exponential decay factor $\Delta\tau$ on amplitude diminished with time. It can be assumed that the complete solution will be considered to be numerically

equal to the steady state solution when their ratio reaches some value η_1 for an increase and η_2 for a decrease in rate of turn. If $\pm Z$ is the ratio of the final to the initial rate of turn, + or - implying that the final and initial rate of turn are in the same and opposite directions respectively, the previous statement can be expressed as:-

$$\left.\begin{array}{ll} \text{For } Z>1 & |\theta_2|_{\text{complete sol}^n} \geq \eta_1 |\theta_2|_{\text{steady state sol}^n} \\ Z<1 & |\theta_2|_{\text{complete sol}^n} \leq \eta_2 |\theta_2|_{\text{steady state sol}^n} \end{array}\right\} \quad (47)$$

For the increased rate of turn case, equation (47) becomes:-

$$e^{-\delta\tau}\left[\frac{\omega_n}{p}(T_1 - T_2)\sin p\tau\right] + T_2 \sin \omega_n \tau \geq \eta_1 T_2 \sin \omega_n \tau \qquad (48)$$

With the range of parameters encountered in the present torsion gyro the damped and undamped natural frequencies can be considered to be numerically equal. However, after a sufficient number of cycles the phase change between those two frequencies could be considerable. The time required for the transient response to reduce by a given amount depends upon amplitude and any phase change can be neglected. Equation (48) then reduces to:-

$$e^{-\delta\tau}(T_1 - T_2) + T_2 \geq \eta_1 T_2 \qquad (49)$$

giving for $Z>1$

$$\tau \leq \frac{1}{\delta} \log_e \left[\frac{Z-1}{Z(1-\eta_1)}\right] \qquad (50)$$

Correspondingly for $Z<1$

$$\tau \geq \frac{1}{\delta} \log_e \left[\frac{1-Z}{Z(\eta_2 - 1)}\right] \qquad (51)$$

With a realistic value of $\Delta = 0.92$, Figure 8 shows, from equations (50) and (51), the variation in the time required for the output to be within 1% (solid curves) and 10% (dotted curves) of the steady state output pertaining to the final rate of turn Ω'.

The step function which gives no inoperative time due to the transient condition can, for positive values of Z, be found from equations (50) and (51). This occurs when the value of the number within the square brackets is equal to unity, giving the condition that $\tau = 0$ when $Z = \frac{1}{\eta}$.

For values of Z between $\frac{1}{\eta_1}$ and $\frac{1}{\eta_2}$ there is no inoperative time. This can be seen from the physical sense, because the step functions between these limits do not increase the final steady state solution beyond the tolerances of η.

For large values of Z the curves are seen to be asymptotes to a constant interval of time. In this case equations (50) and (51) become independent of Z and the time for the transient response to be considered negligible can then be simplified to:

$$\tau = \frac{1}{\Delta} \log_e \left(\frac{1}{1 \pm \eta} \right) \qquad (52)$$

The condition when the final rate of turn approaches zero (i.e. $Z \to 0$) can be seen to give a transient time approaching infinity. However, the

FIGURE 8

INSTRUMENT INOPERATIVE TIME DUE TO TRANSIENT EFFECT.

$$Z = \frac{T_2}{T_1} = \frac{\Omega'}{\Omega}$$

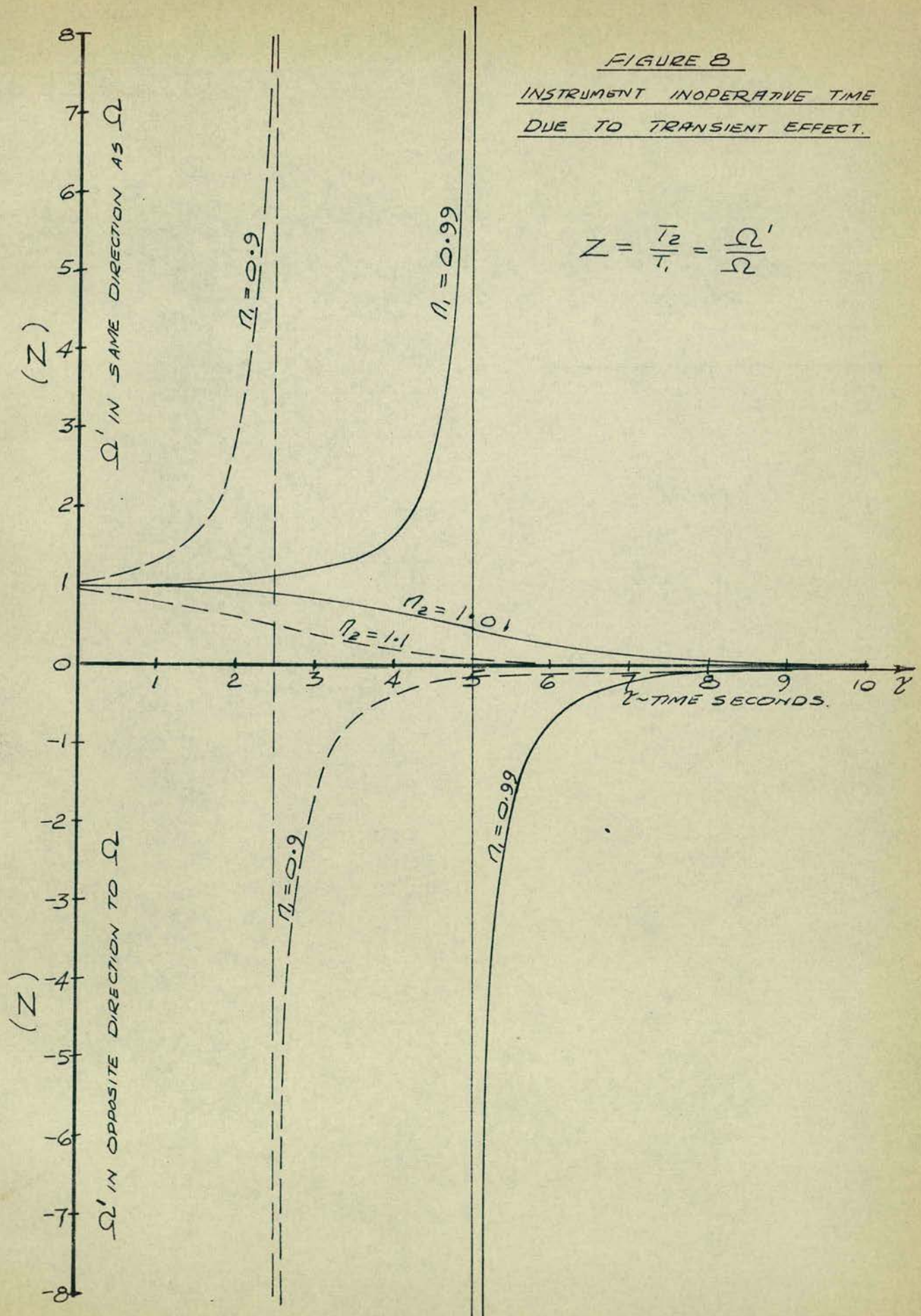

sensitivity of the instrumentation will not record ouputs below a certain value.

The consequences of this delay in recording changes in input could be a serious limitation on this instrument as a rate of turn indicator. Arrangements to overcome this difficulty either by increasing the frequency or damping are impracticable due to other considerations.

CHAPTER 4

4.0 Torsion Gyro - Effects of Unbalance

Any form of unbalance in the system, which induces a torque about the output axis, imposes limitations on the sensitivity and reliability of the instrument. Unbalance within the system can produce output signals either in-phase, or 90° out of phase with the applied rate of turn signal. It is the out of phase signals which are considered to have the most detrimental effect upon the sensitivity of the instrument. This can be seen from figure 3 (Page 89), where the in-phase signals merely shift the intersection of the output and rate of turn axis, whereas, the out of phase signals alter the output/rate of turn relationship.

The principal forms of unbalance in this system which cause the out of phase signals are, the tilting of the rotor axis relative to the output axis and an unbalanced mass attached to the rotor. These effects can be produced by errors in manufacture, or in the case of the unbalanced mass, by the lack of homogenity in the rotor material. The in-phase, unbalanced signals can be caused in this present system by misalignment of the conductors inserted at the periphery of the rotor or, to a lesser extent, by the reaction torque developed as a result of the tilt of the rotor axis relative to the output axis.

The output obtained from an applied rate of

turn is in-phase with the reference rotor drive signal at the tuned resonant condition. It would appear, therefore, that the signals due to unbalance which are not in-phase with the rate of turn signal could be neglected by measuring the output from the system by a phase-sensitive voltmeter, thereby recording only the in-phase signals. However, to achieve maximum sensitivity, the system is operated at the coupled resonant condition. Phase of the output relative to the reference rotor drive signal can not be relied upon, both from the considerations of the small drift from the resonant frequency during operation and the condition discussed on page (51), where it is shown that the tuned resonant condition can never be achieved with unbalance present. A suitable servomechanism could be designed to maintain this phase shift to within a few degrees.

The present investigation is concerned with the effects of unbalance in the system which appear as constant outputs. Rate of turn signals smaller than the out of phase unbalance signals can not be detected and provision must be made to reduce these to an absolute minimum.

The remainder of this chapter discusses each of the effects of unbalance separately and some of the aspects arising out of them.

4.1 Rotor Axis Tilted Towards the Output Axis

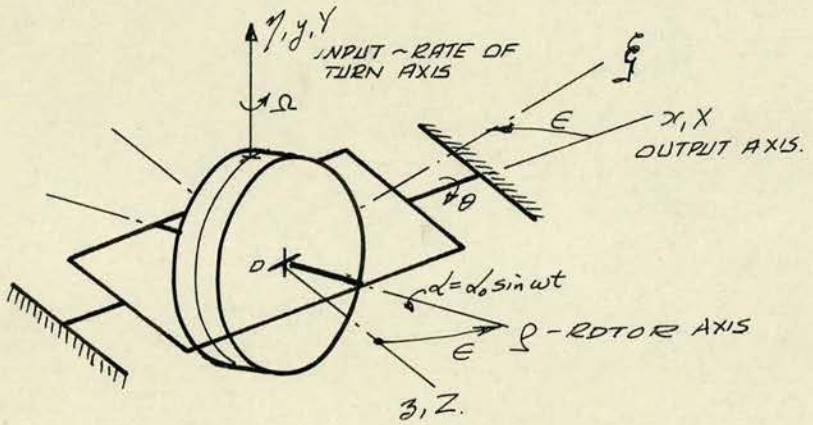

FIG. 9.

Figure 9 shows a diagrammatic arrangement of the instrument with the rotor axis tilted towards the output axis. The orthogonal axes $OXYZ$ are considered attached to the base of the instrument, $Oxyz$ to the gimbal and $O\xi\eta\zeta$ to the rotor. $Oxyz$ coincides with $OXYZ$ and $O\xi\eta\zeta$ when the output amplitude θ and the angle of tilt ϵ are respectively equal to zero. Assume as a first approximation that the rate of turn is applied about input Y-axis and the outer gimbal system is constrained to oscillate torsionally about the x-output axis only. This can be achieved by ensuring that a bending natural frequency of the system does not lie within the operating torsional frequency range and that the gimbals are of rigid construction. By considering θ, α and ϵ to be small displacements the angular velocities of the system can be resolved as:-

$$\left.\begin{aligned}
&\text{Instrument angular velocity } \bar{\Omega} = \Omega\bar{J} \\
&\text{Gimbal angular velocity } \bar{\omega} = \dot{\theta}\bar{\imath} + \Omega\bar{J} - \Omega\theta\bar{k} \\
&\text{Rotor angular velocity} = (\dot{\theta} + \Omega\theta\epsilon)\bar{\imath}' + \Omega\bar{J}' + (\dot{\alpha} + \dot{\theta}\epsilon - \Omega\theta)\bar{k}' \\
&\qquad\qquad = (\dot{\theta} + \dot{\alpha}\epsilon)\bar{\imath} + \Omega\bar{J} + (\dot{\alpha} - \Omega\theta)\bar{k}
\end{aligned}\right\} \quad (53)$$

where $\bar{J}$ is a unit vector along the OY axis and $\bar{\imath}, \bar{J}, \bar{k}$ and $\bar{\imath}', \bar{J}', \bar{k}'$ are unit vectors along the respective $Oxyz$ and $O\xi\eta\zeta$ orthogonal axes. With A, B and C referring to the moments of inertia of the system about the orthogonal axes, which, when included with the subscripts 'i' and 'o' refer only to the inner rotor and outer gimbal system respectively.

The rotor angular momentum about the $O\xi\eta\zeta$ axes, can be expressed as:-

$$\bar{h} = A_i(\dot{\theta} + \Omega\theta\epsilon)\bar{\imath}' + (B_i\Omega)\bar{J}' + C_i(\dot{\alpha} - \Omega\theta + \dot{\theta}\epsilon)\bar{k}' \qquad (54)$$

From the angular momentum equations, the torque about the x-axis can be indicated in terms of the rotor angular momentum and angular velocity of the rotating $Oxyz$ axes,

$$\omega\,\bar{\imath}_{x'} = \dot{h}_x - h_y\omega_z + h_z\omega_y \qquad (55)$$

where h_x, h_y and h_z are the components of the angular momentum, expressed in equation (54), about the x, y and z axes and ω_y and ω_z are components of the gimbal angular velocity expressed in equation (53). With a constant rate of turn (Ω) applied about the OY axis (i.e. $\dot{\omega}_y = 0$) the torque about the x-axis due to the inertia of the inner system can be found by substituting equations (53) and (54) into equation (55).

$$\therefore T_x' = [A_1(\ddot{\theta} + \Omega\dot{\theta}\epsilon) + C_1(\ddot{\alpha} - \Omega\dot{\theta} + \ddot{\theta}\epsilon)\epsilon] - [(B_1\Omega)(-\Omega\theta)]$$

$$+ [C_1(\dot{\alpha} - \Omega\theta + \dot{\theta}\epsilon) - A_1\epsilon(\dot{\theta} + \Omega\theta\epsilon)]\Omega \qquad \text{——————(56)}$$

The torque, due to the inertia of the gimbal or outer system, can also be found by these equations:-

$$\therefore T_{x_0} = A_0\ddot{\theta} + (B_0 - C_0)(\Omega^2\theta) \qquad \text{——————(57)}$$

By combining equations (56) and (57), the total torque about the output x-axis can be obtained and equated to the sum of the damping and spring torques.

$$\therefore T_x = [A + C_1\epsilon^2]\ddot{\theta} + \Omega^2[(B-C) - A_1\epsilon^2]\theta + \ddot{\alpha}(C_1\epsilon) + \dot{\alpha}(C_1\Omega)$$

$$= -k_x\theta - C_x\dot{\theta} \qquad \text{——————(58)}$$

where k_x and C_x are the stiffness and damping co-efficients of the gimbal system about the output x-axis. By neglecting second order effects and eliminating small terms, i.e. $[C_1\epsilon^2 \ll A]$ and $\Omega^2\{(B-C) - A_1\epsilon^2\} \ll k_x$ equation (58) reduces to:-

$$A\ddot{\theta} + C_x\dot{\theta} + k_x\theta = -C_1\ddot{\alpha}\epsilon - C_1\dot{\alpha}\Omega \qquad \text{——————(59)}$$

Equation (59) is, with the exception of the first term of the right hand side, the same as equation (24) which was derived for the balanced system. This shows that the effect of this unbalance is to produce an additional forcing term proportional to the component of the inertia of the rotor about the output axis. With constant co-efficients and a sinusoidal input $\alpha = \alpha_0 \sin\omega t$, the steady state solution to equation (59) becomes:-

$$\theta = \frac{\alpha_0\omega C_1}{A\sqrt{(\omega_n^2 - \omega^2)^2 + \left(\frac{C_x\omega}{A}\right)^2}}\left[\omega\epsilon\sin(\omega t - \phi) - \Omega\cos(\omega t - \phi)\right] \qquad \text{——(60)}$$

ω_n represents the undamped natural frequency of the gimbal system about the output shafts and ω is the forcing frequency of the system. The phase angle ϕ equal to $\tan^{-1}\frac{\omega C_x}{A(\omega_n^2-\omega^2)}$ determines the phase of the output relative to the rotor amplitude $\alpha = \alpha_0 \sin \omega t$

Equation (60) can be expressed in its non-dimensional form by substituting f, the frequency ratio equal to ω/ω_n and d the damping ratio equal to C_x/C_c

$$\theta = \frac{\alpha_0 f C_1}{A\omega_n\sqrt{(1-f^2)^2+(2df)^2}}\left[\omega\epsilon\sin(\omega t-\phi) - \Omega\cos(\omega t-\phi)\right] \quad (61)$$

It can be seen from equation (61) that the output, induced by the tilt of the rotor axis, is 90^0 out of phase with the output obtained from an applied rate of turn Ω .

4.2 Unbalanced Mass Attached to the 'Rotor'

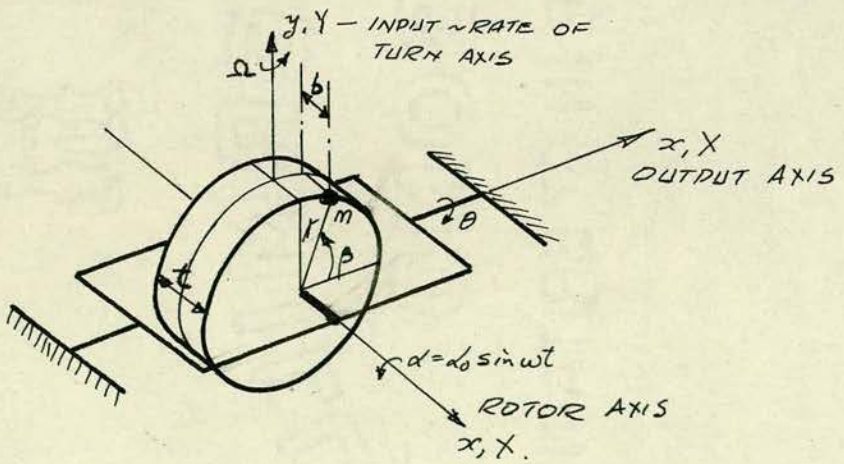

FIG. 10.

Figure (10) shows the diagrammatic arrangement of the

instrument with the orthogonal axes $OXYZ$ and $Oxyz$ considered attached to the base of the instrument and the gimbal respectively. As in the previous case, these two orthogonal axes are concurrent when the output oscillation θ is zero. An unbalanced mass is considered to be attached to the rotor at an angle of β from the xoz plane and displaced by a distance b from the oy axis. This unbalanced mass represents the effect produced by small manufacturing errors or the lack of homogenity in the 'rotor' material, which will locate the unbalance mass at any point within the rotor.

As in the previous case, it is assumed that the rate of turn is applied about the Y-axis and the outer gimbal system oscillates in torsion about the x-output axis only.

By considering θ and α to be small angular displacements, the angular velocities about the orthogonal axes can be resolved, as in Chapter 3.1, for the system without the unbalance mass.

i.e. Instrument angular velocity $\bar{\Omega} = \Omega\bar{J}$

Gimbal angular velocity $\bar{\omega} = \dot{\theta}\bar{\imath} + \Omega\bar{J} - \Omega\theta\bar{k}$

Rotor angular velocity $= \dot{\theta}\bar{\imath} + \Omega\bar{J} + (\dot{\alpha} - \Omega\theta)\bar{k}$ } (62)

These angular velocities, together with the inertia of the system, give from the angular momentum equations, a torque about the x-output axis.

$$\therefore T_x = \dot{h}_x - h_y\omega_z + h_z\omega_y \qquad (63)$$

The unbalanced mass also gives a torque about this axis, which, from D'Alamberts principle, is equal to the product of its mass and its acceleration about the x-axis. This acceleration can be resolved into its x, y, z components,

$$\therefore T_{mx} = m(y\bar{a}_z - z\bar{a}_y) \qquad (64)$$

where T_{mx} is the torque about the x-axis due to the unbalanced mass and m is the unbalanced mass. The co-ordinates of the mass are y and z and the accelerations of the mass about these co-ordinates are $\bar{a}_y$ and $\bar{a}_z$.

The total torque about the x-axis can then be found by summing equations (63) and (64). This torque can also be equated to the sum of the spring and damping torques about the output shafts,

$$\therefore \dot{h}_x - h_y\omega_z + h_z\omega_y + T_{mx} = -C_x\dot{\theta} - k_x\theta \qquad (65)$$

where, neglecting out of balance effects, h_x, h_y and h_z refer to the angular momentum about the x, y and z axes.

Consider A, B and C to be the inertias of the balanced system about the x, y and z axes, which, when included with the subscript 'c' refers to the inner rotor system only. Assume the x, y and z axes to be principal axes for the balanced system, then the components of the angular momentum about the x, y and z axes are:-

$$h_x = A\omega_x \quad , \quad h_y = B\omega_y \quad , \quad h_z = C\omega_z \qquad (66)$$

where ω_x, ω_y and ω_z are the components of the angular rotation of the orthogonal axes $Oxyz$. Equation (65) can therefore be expanded by substituting equations (64) and (66)

$$\therefore A\ddot{\theta} + (B-C)\Omega^2\theta + C_1\dot{\alpha}\Omega + T_{mx} = -C_x\dot{\theta} - k_x\theta \qquad \text{——(67)}$$

In a practical system $k_x\theta$ will be very much greater than $(B-C)\Omega^2\theta$. The latter can therefore be neglected to give:-

$$A\ddot{\theta} + C_x\dot{\theta} + k_x\theta + T_{mx} + C_1\dot{\alpha}\Omega = 0 \qquad \text{——(68)}$$

The torque T_{mx} due to the unbalanced mass is evaluated from equation (64), the displacements along the x, y and z axes being:-

$$\left.\begin{aligned} x &= r\cos\beta \\ y &= r\sin\beta \\ z &= b = \text{constant} \end{aligned}\right\} \quad (69)$$

where r = radius of unbalanced mass about the oz axis

$\beta = \lambda + \alpha$ = rotational displacement of the mass about the oz axis

λ = mean displacement

α = additional displacement due to the input oscillations

b = displacement of mass from the xoy plane.

It can be shown that the absolute velocities and accelerations of a moving point are:-

$$\left.\begin{aligned} \bar{V}_x &= \dot{x} - \omega_z y + \omega_y z \\ &\text{etc} \end{aligned}\right. \qquad \left.\begin{aligned} \bar{a}_x &= \dot{V}_x - \omega_z V_y + \omega_y V_z \\ &\text{etc} \end{aligned}\right\} \quad (70)$$

By considering a constant applied rate of turn Ω, i.e. $\dot{\omega}_y = 0$ the torque, due to this unbalanced mass, becomes

from equations (64), (69) and (70):-

$$T_{mx} = m\Big[\{b^2+r^2\sin^2\beta\}\ddot{\theta} + \{r^2\sin 2\beta\dot{\alpha}\}\dot{\theta} + \theta\{\Omega^2(b^2-r^2\sin^2\beta) - 2\Omega br\sin\beta\dot{\alpha}\}$$
$$+\theta^2\{\Omega^2 br\sin\beta\} - \dot{\theta}\theta\{\Omega r^2\sin 2\beta\} - \Omega^2\{br\sin\beta\} + \Omega\{2r^2\sin^2\beta\dot{\alpha}\}$$
$$+ br\sin\beta\dot{\alpha}^2 - br\cos\beta\ddot{\alpha}\Big] \qquad \text{——————(71)}$$

By neglecting second order terms and eliminating small terms, ie $\Omega^2(b^2-r^2\sin^2\beta) \ll k_x$, equation (71) can be simplified and substituted into equation (68) to give:-

$$A'\ddot{\theta} + C_x\dot{\theta} + k_x\theta = -C_1\dot{\alpha}\Omega + mbr\Omega^2\sin\beta - 2mr^2\Omega\sin^2\beta\dot{\alpha}$$
$$-mbr\sin\beta\dot{\alpha}^2 + mbr\cos\beta\ddot{\alpha} \qquad \text{——————(72)}$$

where $A' = A + m(b^2+r^2\sin^2\beta)$

i.e. A' is the sum of the inertia of the balanced system and the inertia of the unbalanced mass (assuming β is approximately constant) about the x-axis.

The steady state solution of equation (72) can be found by summing the individual solutions obtained by considering the right hand side to be a linear equation with constant coefficients and having several forcing functions.

$$\theta = -\Big[C_1 + 2mr^2\sin^2\beta\Big]\frac{\alpha_0 f\Omega\cos(\omega t-\phi)}{A\omega_n\sqrt{(1-f^2)^2+(2fd)^2}}$$
$$-\frac{mf^2br\alpha_0\cos\beta\sin(\omega t-\phi)}{A\sqrt{(1-f^2)^2+(2fd)^2}}$$
$$-\frac{mbr\alpha_0^2f^2\sin\beta}{2A}\left[1 + \frac{\cos(2\omega t-\sigma)}{\sqrt{(1-4f^2)^2+(4fd)^2}}\right]$$
$$+\frac{m\Omega^2br\sin\beta}{A\omega_n^2} \qquad \text{——————(73)}$$

Equation (73) is given in its non dimensional form where:-

ω = operating torsional frequency

ω_n = undamped torsional natural frequency

f = frequency ratio = ω/ω_n

d = damping ratio = $C_x/2A\omega_n$

ϕ = phase angle = $\tan^{-1}\frac{2fd}{1-f^2}$

σ = phase angle = $\tan^{-1}\frac{4fd}{1-4f^2}$

With the operating frequency approximately equal to the undamped natural frequency, constant outputs and outputs at twice the forcing frequency are negligible compared to the output at the forcing frequency.

Equation (73) can therefore be approximated to:

$$\theta = -\left[C_1 + 2Mr^2\sin^2\beta\right]\frac{\alpha_0 f\,\Omega\cos(\omega t-\phi)}{A\omega_n\sqrt{(1-f^2)^2+(2fd)^2}} - \frac{mf^2 br\alpha_0\cos\beta\sin(\omega t-\phi)}{A\sqrt{(1-f^2)^2+(2df)^2}} \qquad (74)$$

With a moderate unbalanced mass in the system $C_1 \gg 2Mr^2\sin^2\beta$ the output due to the unbalanced mass can then be further reduced to:-

$$\theta = -\left[C_1\Omega\cos(\omega t-\phi) + mbr\omega\cos\beta\sin(\omega t-\phi)\right]\frac{\alpha_0 f}{A\omega_n\sqrt{(1-f^2)^2+(2fd)^2}} \qquad (75)$$

The error signal proportional to the unbalanced mass m can be seen from equation (75) to be, as in the previous case, 90° out of phase with the output obtained from an applied rate of turn Ω.

4.3 Unbalance in the Drive System

The present experimental instrument has, as part of the electro-magnetic drive system, a number of conductors placed across the periphery of the rotor. Excitation is achieved in a direction at right angles to those conductors and to the lines of magnetic flux passing through the rotor.

When the conductors are not aligned parallel to the rotor shafts, a torque can be induced about axes other than the rotor axis. If a component of this unbalanced torque acts about the output x-axis an error signal is established.

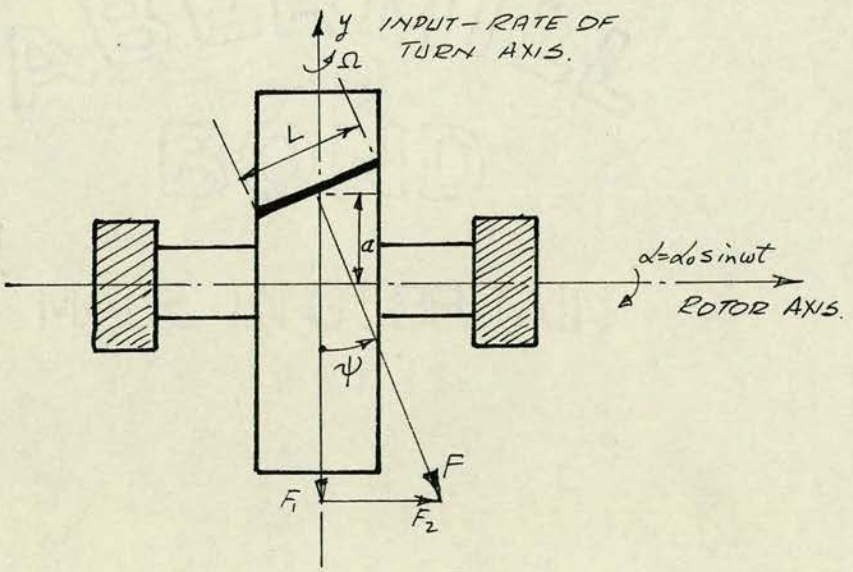

FIG. 11.

Figure 11 illustrates a section through the gimbal, normal to the output x-axis. A conductor is

shown set at an angle ψ to the rotor axis and displaced by a vertical distance, a'

where $a = a_0 + \alpha_0 \sin \omega t$ ——————— (76)

a_0 is a constant displacement and $\alpha_0 \sin \omega t$ is the amplitude of the rotor oscillation superimposed upon a_0

The driving force F acts normal to the conductor. Its amplitude can be derived from the characteristic electro magnetic force equation,

$$F = BLI \quad \text{——————} \quad (77)$$

where B is the flux density, L the length of the conductor and $I = i \cos \omega t$ the current supplied to the conductor.

This force can be resolved into components F_1 and F_2 parallel to the oy and oz axes respectively. The force F_1 is the normal driving force which develops the torque about the rotor axis. The force F_2 is displaced by the distance a' from the x-axis and therefore develops a torque T_x about this axis.

i.e. $T_x = F_2 \times a = (BLi \cos \omega t \sin \psi) \times (a_0 + \alpha_0 \sin \omega t)$

$\therefore T_x = -BLi a_0 \sin \psi \cos \omega t - \frac{1}{2} BLi \alpha_0 \sin \psi \sin 2\omega t$ } (78)

This torque will act as a forcing function on the outer gimbal system to give a differential equation of motion, of the form:-

$$A\ddot{\theta} + C_x \dot{\theta} + k_x \theta = -BLi a_0 \sin \psi \cos \omega t - \tfrac{1}{2} BLi \alpha_0 \sin \psi \sin 2\omega t \quad \text{——} (79)$$

Since the system is operated at its fundamental undamped natural frequency the second

forcing function of equation (79) can be considered negligible compared to the first forcing function. A steady state solution to this equation can then be obtained, i.e.

$$\theta = \frac{-BLi\, a_0 \sin\psi \cos(\omega t - \phi)}{A\omega_n^2\left[(1-f^2)^2 + (2df)^2\right]} \qquad (80)$$

where f and d are the non-dimensional frequency and damping coefficients and ω_n is the undamped natural frequency of the gimbal system about the output shafts.

It can be seen by comparing equations (26) and (80) that this error signal is in phase with the output obtained with an applied rate of turn signal Ω.

This analysis considers only one unbalanced conductor. The experimental instrument has six conductors all of which may have, to a certain extent, this form of unbalance. The resultant of the effects from all the unbalanced conductors would have to be determined to obtain realistic values due to this effect. This is experimentally outwith the scope of the present work. However, the variation in this signal by altering the distance 'a' has been investigated and the results obtained are shown in Chapter 10.

4.4 Torque Reaction

As a part of the drive system of this instrument, magnets are attached to the gimbal adjacent to the periphery of the rotor. These magnets, together with the conductors placed across the periphery of the rotor, cause a torque to be induced in the rotor. A corresponding reaction torque is therefore applied to the magnets. In a balanced system this reaction torque has no effect upon the output, provided a bending natural frequency of the system does not fall within the range of the operating torsional frequency. However, with an unbalance present, as discussed previously in paragraph 4.1, where the rotor axis is tilted with respect to the output axis, the applied torque does not act at right angles to the output axis. A torque can therefore be induced about the output x-axis

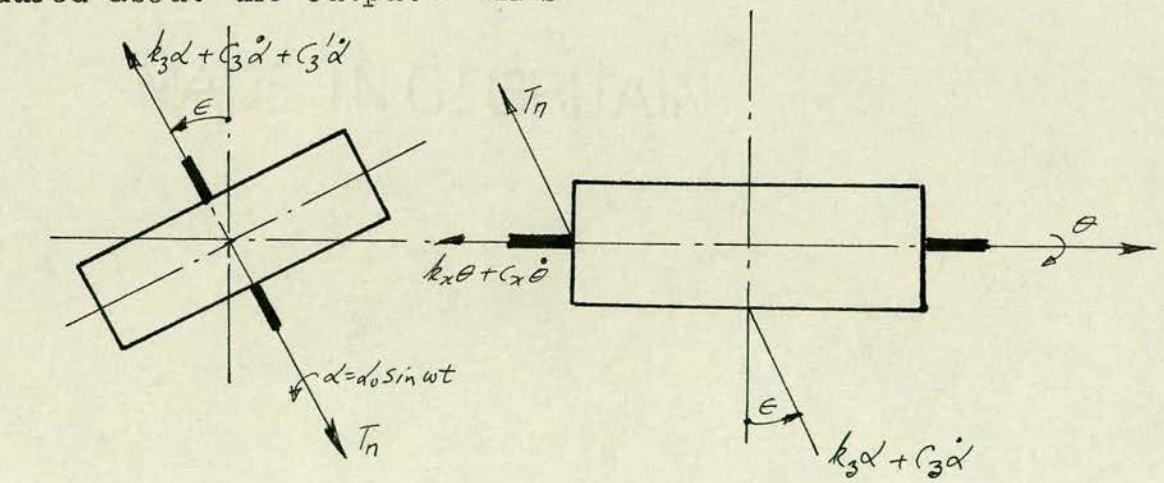

FIG. 12.

Figure 12 shows the torques acting on the inner rotor

and outer gimbal systems. k_x and k_z are the stiffness coefficients and C_x and C_z the internal damping coefficients of the outer and inner systems about their axes. C_z' is the external damping coefficient of the inner system and is assumed, for the purpose of this analysis, to be proportional to the input velocity $\dot{\alpha}$.

The equation of motion of the inner rotor system is therefore:-

$$C\ddot{\alpha} = T_n - k_z\alpha - C_z\dot{\alpha} - C_z'\dot{\alpha} \qquad (81)$$

where C is the moment of inertia of the rotor about the rotor shafts and T_n is the torque induced normal to the rotor shaft.

For the outer gimbal system, the reaction torques are applied at the magnets, the stiffness and internal damping torques applied to the rotor drive are opposed by an equal and opposite torque applied to the gimbal at the rotor shafts. The equation of motion of the outer gimbal system is therefore:-

$$A\ddot{\theta} = (k_z\alpha + C_z\dot{\alpha})\sin\epsilon - T_n\sin\epsilon - k_x\theta - C_x\dot{\theta} \qquad (82)$$

Consider the axis tilt to be small and substitute the value of T_n obtained from equation (81) in equation (82), then:-

$$A\ddot{\theta} + C_x\dot{\theta} + k_x\theta = -C\ddot{\alpha}\epsilon - C_z'\dot{\alpha}\epsilon \qquad (83)$$

As this analysis is an alternative method to the analysis of paragraph 4.1, the first forcing term of equation (83) is discussed in this section. The

second forcing function gives a steady state solution

$$\theta = -\frac{C_3' \alpha_0 f \epsilon \cos(\omega t - \phi)}{A\omega_n \sqrt{(1-f^2)^2 + (2fd)^2}} \qquad (84)$$

The symbols of this equation are similar to those detailed for equation (61).

It can be seen from equation (84) that the signal obtained from this torque reaction creates an output, in phase with, but independent of, the applied rate of turn Ω. With the parameters of the present system, this unbalanced effect can be considered negligible compared to those previously discussed.

4.5 Combined Effects of Unbalance

The combined effects of the unbalance and rate of turn signals are summarized from equations (61), (75), (79) and (84), to give a peak output of:

$$\theta_o = \frac{\alpha_0 f}{A\omega_n \sqrt{(1-f^2)^2 + (2fd)^2}} \left(\sqrt{X^2 + Y^2} \right) \qquad (85)$$

where
$$X = -\left[C_1 \Omega + C_3' \epsilon + \frac{BLi\, a_0 \sin\psi}{\alpha_0 \omega} \right] \cos(\omega t - \phi)$$
$$Y = \left[C_1 \epsilon - mbr \cos\beta \right] \omega \sin(\omega t - \phi) \qquad (86)$$

where X and Y are the resultant of the in-phase and 90° out of phase output signals respectively. With the small values of axis tilt and external damping coefficients encountered in the present instrument the output proportional to $C_3' \epsilon$ will be less than an equivalent rate of turn of 0.2 r.p.m., which does not

greatly influence the present system. However, this would have to be reduced considerably in a more accurate instrument. The other output in phase with a rate of turn signal is entirely due to the drive system and a replacement of this type of excitation would obviate this difficulty.

Two of the main forms of unbalance in this system are, the tilt of the rotor axis and the unbalanced mass attached to the rotor. However, as the outputs from these effects are in-phase, any inherent unbalance induced during manufacture could be minimized by deliberate unbalance introduced to the system. In the present instrument difficulty was experienced in aligning the rotor shafts precisely at right angles to the output shafts. Unbalanced masses were therefore added to the face of the rotor to reduce the resultant effect of this form of unbalance. Rough balance was carried out at an angle of $\beta = 0^\circ$ and finer balance carried out with β approaching 90°, as the effectiveness of adding mass at this point is considerably reduced.

This procedure, together with experimental results of the above unbalanced effects, are given in Chapter 10.

4.6 Coupling Effects due to Unbalance

With no applied rate of turn, the balanced torsion gyro can be considered as two single degree of freedom systems, acting about the input and output shafts. With mass unbalance or a tilt of the input axis, coupling between the two systems can be set up.

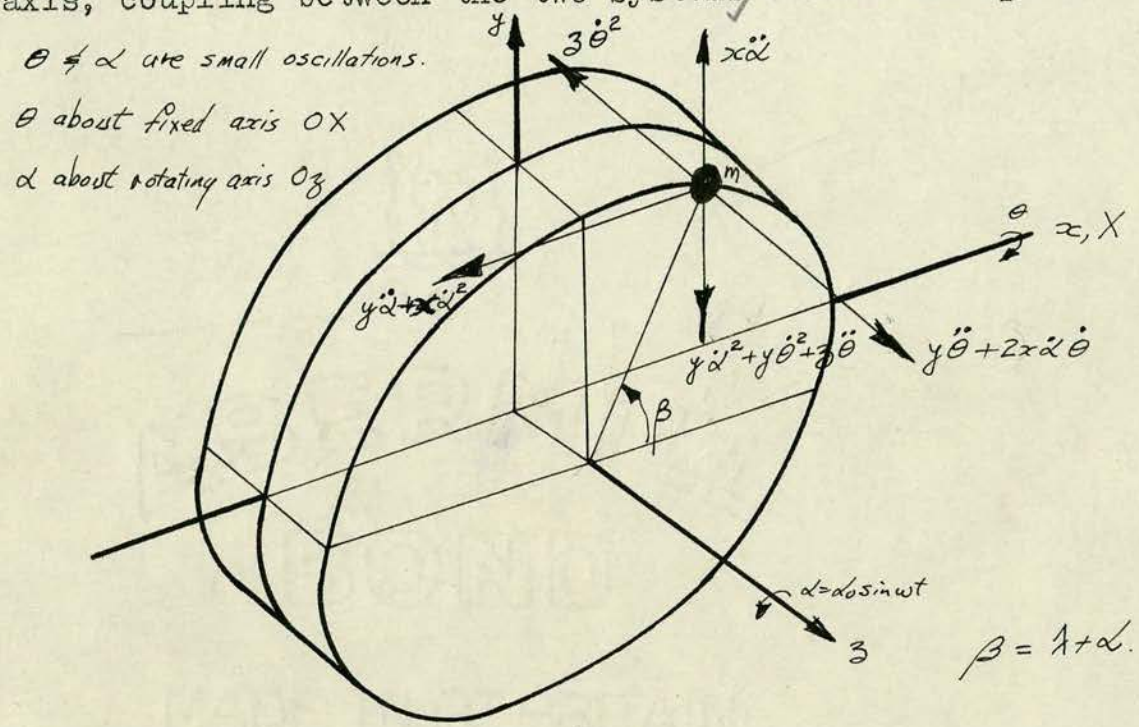

FIG 13.

Figure 13 shows the accelerations of the unbalanced mass due to the rotor and gimbal oscillations. These accelerations, together with the unbalanced mass, give the torques T_{mx} and T_{mz} about the x and z-axis.

$$\therefore T_{mx} = m[\ddot{\theta}(y^2+z^2) + 2xy\dot{\alpha}\dot{\theta} + yz\dot{\alpha}^2 - xz\ddot{\alpha}] \qquad (87)$$

$$T_{mz} = m[\ddot{\alpha}(x^2+y^2) - xy\dot{\theta}^2 - xz\ddot{\theta}] \qquad (88)$$

The total torque acting about the x and z-axis can then be found by adding these torques to the torques for the balanced system, i.e.

$$[A + m(y^2+z^2)]\ddot{\theta} + [C_x + 2mxy\dot{\alpha}]\dot{\theta} + k_x\theta = mxz\ddot{\alpha} - myz\dot{\alpha}^2 \qquad (89)$$

$$[C_1 + m(x^2+y^2)]\ddot{\alpha} + C_z\dot{\alpha} + k_z\alpha = mxz\ddot{\theta} + mxy\dot{\theta}^2 \qquad (90)$$

When operating at the resonant condition, the second forcing terms of the above equations provide a constant output and an output at twice the operating frequency. These terms can be neglected compared with the magnitude of the output from the first forcing term.

By neglecting damping and considering the unbalance to be small, equations (89) and (90) become:-

$$A\ddot{\theta} + k_x\theta = mxz\ddot{\alpha} \qquad (91)$$

$$C_1\ddot{\alpha} + k_z\alpha = mxz\ddot{\theta} \qquad (92)$$

With an unbalance due to axis tilt, similar equations to (91) and (92) can be obtained from the analysis of 4.1

$$A\ddot{\theta} + k_x\theta = -C_1\epsilon\ddot{\alpha} \qquad (93)$$

$$C_1\ddot{\alpha} + k_z\alpha = -C_1\epsilon\ddot{\theta} \qquad (94)$$

Equations (91) to (94) can then be compounded to give:-

$$\ddot{\theta} + p_1^2\theta = a\ddot{\alpha} \qquad (95)$$

$$\ddot{\alpha} + p_2^2\alpha = b\ddot{\theta} \qquad (96)$$

where $a = \dfrac{mxz - C_1\epsilon}{A}$

$b = \dfrac{mxz - C_1\epsilon}{C_1}$

p_1 = gimbal undamped natural frequency $= \sqrt{k_x/A}$

p_2 = rotor undamped natural frequency $= \sqrt{k_z/C_1}$

From equations (95) and (96) it can be seen that the two systems are independent only when a and b are equal to zero; that is when the system is in its

balanced state.

By assuming a sinusoidal output, equations (95) and (96) become:-

$$(p_1^2 - \omega^2)\theta = -a\omega^2\alpha \qquad (97)$$

$$(p_2^2 - \omega^2)\alpha = -b\omega^2\theta \qquad (98)$$

Equation (97) can be equated to show: $\theta = -\frac{a\omega^2\alpha}{p_1^2 - \omega^2}$ which, when substituted in equation (98) gives:-

$$(p_2^2 - \omega^2) = \frac{ab\omega^4}{(p_1^2 - \omega^2)}$$

$$\therefore \omega^4(1-ab) - \omega^2(p_1^2 + p_2^2) + p_1^2 p_2^2 = 0 \qquad (99)$$

With no unbalance present, i.e. a = b = 0, the equation reduces to:-

$$(\omega^2 - p_1^2)(\omega^2 - p_2^2) = 0 \qquad (100)$$

Equation (100) gives two roots,

$$\left.\begin{aligned} \omega_1^2 &= p_1^2 \\ \omega_2^2 &= p_2^2 \end{aligned}\right\} \qquad (101)$$

These roots p_1 and p_2 are the undamped natural frequencies of the gimbal and rotor systems respectively.

Solve equation (99) as a quadratic in ω^2 to obtain:-

$$\omega_{1,2}^2 = \left\{(p_1^2 + p_2^2) \pm \sqrt{(p_1^2 - p_2^2)^2 + 4p_1^2 p_2^2 ab}\right\} \frac{1}{2(1-ab)} \qquad (102)$$

For the condition when p_1 does not equal p_2,

$$\omega_{1,2}^2 = p_1^2\left[1 + \frac{p_1^2 ab}{p_1^2 - p_2^2}\right] \text{ or } p_2^2\left[1 - \frac{p_2^2 ab}{p_1^2 - p_2^2}\right] \qquad (103)$$

provided ab is considered as a small quantity

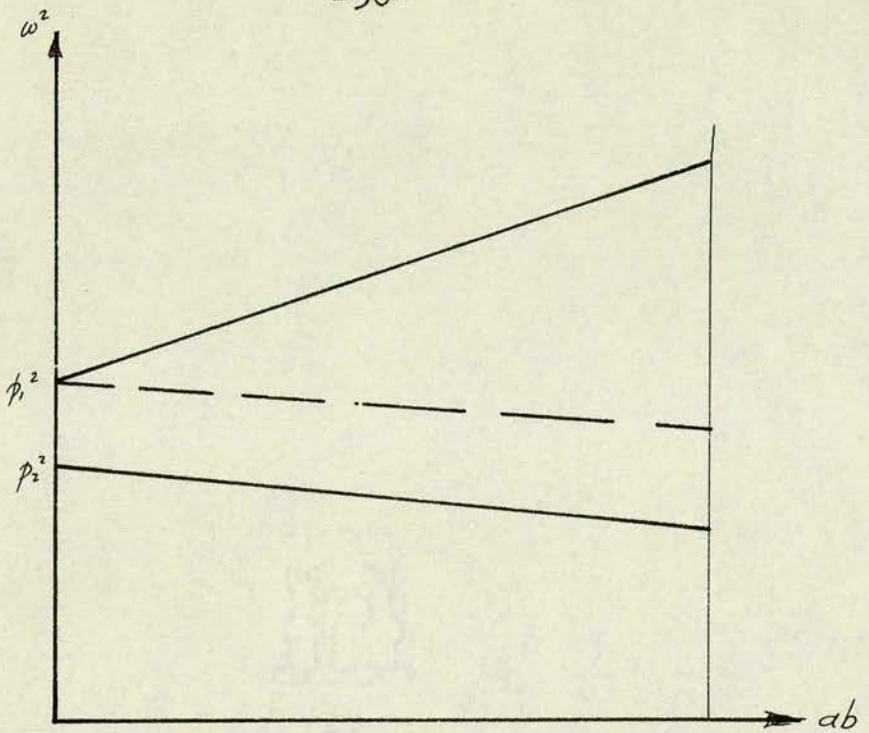

FIG 14

Figure 14 shows the variation of ω^2 with the resultant unbalance ab. The special case of the tuned resonant condition where the natural frequencies of both inner and outer systems are equal can only be realised when the unbalance is zero.

If the system is operated with both the undamped natural frequencies equal to (i.e. $p = p_1 = p_2$) equation (102) can be simplified to:-

$$\frac{\omega^2}{p^2} = \frac{(1 \pm \sqrt{ab})}{1 - ab} \qquad (104)$$

With the frequency ratio $f = \frac{\omega}{p}$ equation (104) can be reduced to:-

$$f = (1 \mp \sqrt{ab})^{-\frac{1}{2}} \qquad (105)$$

By substituting for values of a and b and expanding by the Binomial Theorum, equation (105) becomes:-

$$f = 1 \pm \tfrac{1}{2}\sqrt{\tfrac{C_1}{A}}\,\epsilon \qquad (106)$$

As the angle of tilt ϵ is a small term, second and higher order terms of ϵ can be neglected. The values of C, and A for this instrument can be substituted to give:-

$$f = 1 \pm 0.266\epsilon \qquad (107)$$

When operating at the natural frequency of either the rotor or gimbal system, the response of the other system is reduced unless the two natural frequencies have the same value. This condition can be seen, from this analysis, to occur only when there is no coupling and therefore no unbalance within the system. As the output of the instrument is dependent upon the response of both the rotor and gimbal systems any form of unbalance which causes this coupling reduces the output amplitude considerably.

CHAPTER 5

5.0 Damping

In the analysis previous to this chapter, the damping torque within the system was assumed to be proportional to the velocity of the oscillation, the coefficient of damping C being assumed constant. During tests to ascertain the value of this viscous damping coefficient, it was found that the amplitude did not decay during the free vibration tests in the logarithmic manner contemplated for viscous damping. Further damping tests were therefore carried out to establish the relationship of the damping coefficient to the motion of the system, both for the rotor oscillating inside the gimbal and the gimbal oscillating within the external frame of the instrument.

The method used to determine the rate of decay of the oscillations was that of the free torsional oscillations, in which the system was oscillated at a given amplitude and then released. The decay of the amplitude was then measured by either a variable capacitance or inductance type proximity gauge. The resulting signal, after passing through a frequency modulated circuit, produced a trace of the amplitude on an oscilloscope. By means of an oscilloscope camera having a motor capable of passing the film at a pre-determined speed through the camera, the amplitude of the decaying oscillation, with respect to time, can be

ascertained.

Figure (15) shows an example of the trace obtained. The initial amplitude of the vibration was varied over the stress range encountered during normal operation of the instrument and the damping relationship thereby evaluated. The initial amplitude of vibration was obtained by using two methods, firstly, through oscillating the system with its normal exciting system and, secondly, by means of a mechanical vibrator oscillating at the resonant frequency of the system. The mechanical vibrator was applied at various points of the frame to oscillate the gimbal system about the output shafts and the rotor about its shafts. The point of application was selected to oscillate the system under consideration, in torsion only. This test was carried out for various amplitudes and it was found that the damping corresponding to a given amplitude was constant, regardless of whether this was the initial amplitude or the amplitude obtained during a decaying oscillation.

5.1 Damping Measurement

In the ideal linear free vibrating system of one degree of freedom, the differential equation of motion can be expressed as:-

$$A\ddot{\theta} + C\dot{\theta} + k\theta = 0 \qquad \text{——————} (108)$$

The form of the solution of this equation depends upon

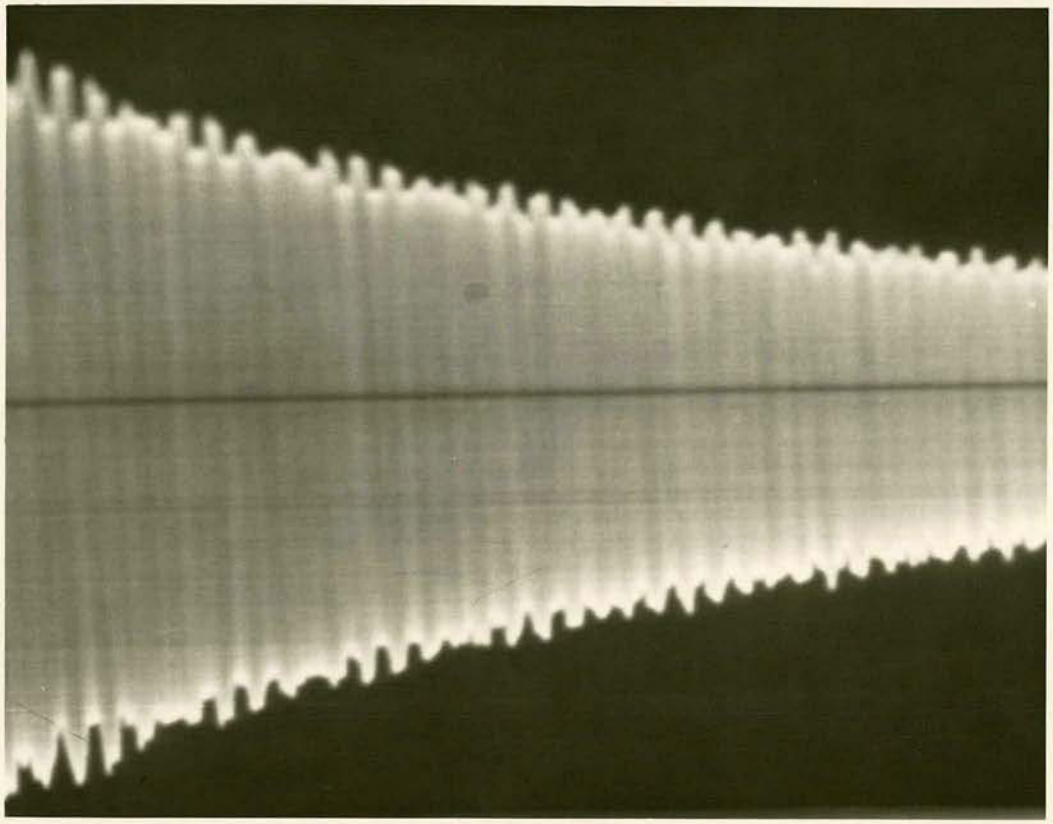

FIG. 15. FREE VIBRATION DAMPING CURVE FOR OUTER SYSTEM.

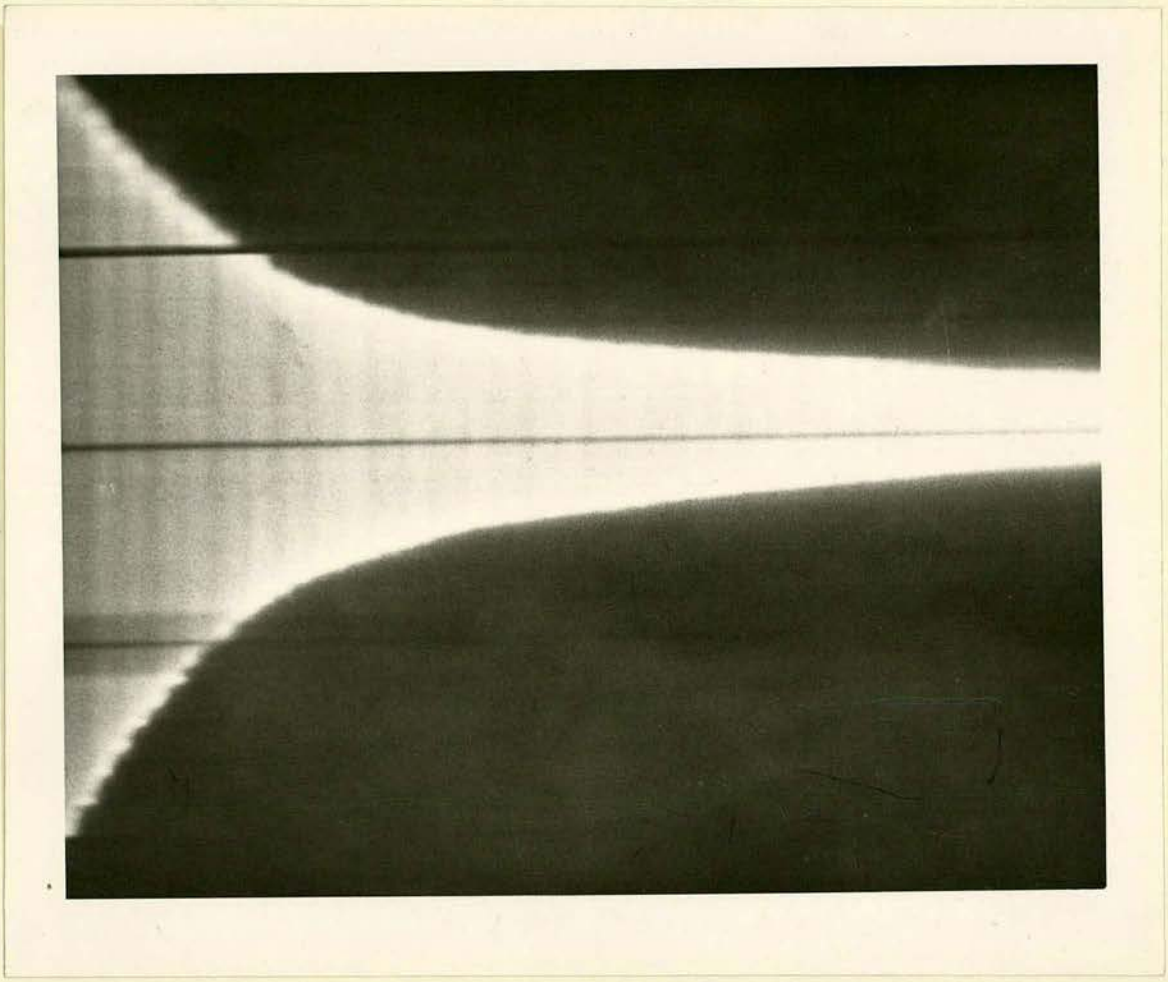

FIG. 16. FREE VIBRATION DAMPING CURVE WITH INDUCED MAGNETISM. OUTER SYSTEM.

the value of C, the coefficient of viscous damping, to the other constants of the system. For small damping as encountered within the present system, i.e. when $\frac{k}{A} > (\frac{c}{2A})^2$, there is a decaying oscillation of circular frequency $p = \sqrt{\omega_n^2 - \Delta^2}$

where $\omega_n = \sqrt{k/A}$ = undamped natural frequency

$\Delta = \frac{c}{2A}$

The solution of equation (108) is then of the form:-

$$\theta = e^{-\Delta t}[A \sin(pt - \sigma)] \qquad (109)$$

where A and σ are arbitrary constants depending upon the initial conditions.

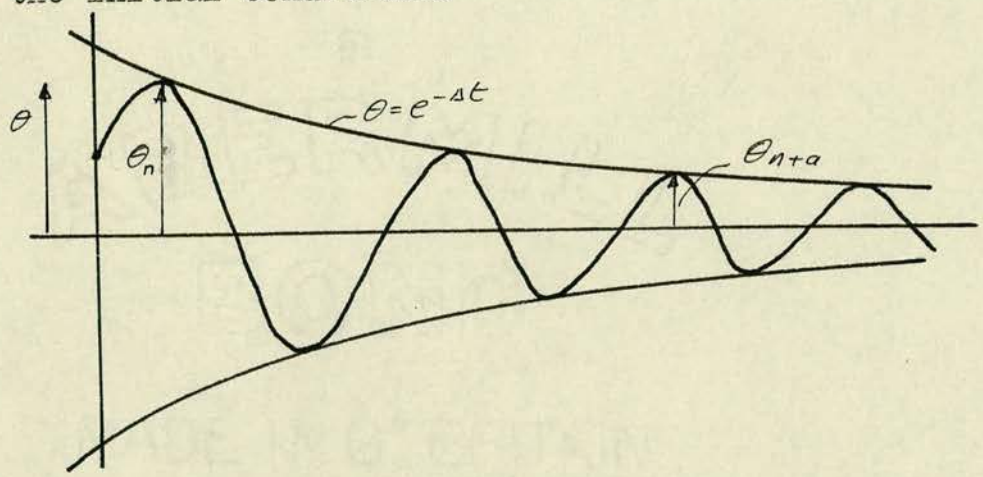

FIG 17.

Figure (17) shows θ as a function of time. The amplitude decreases by a definite percentage each cycle and the natural logarithm of the ratio of two successive amplitudes is called the logarithmic decrement δ

i.e. $\delta = \log_e \frac{\theta_n}{\theta_{n+1}}$ or for an interval

of 'a' cycles $\delta = \frac{1}{a} \log_e \frac{\theta_n}{\theta_{n+a}}$ ——————— (110)

For small damping $\delta = 2\pi d$ The non-dimensional damping coefficient d can then be expressed as:-

$$d = \frac{1}{2\pi a} \log_e \frac{\theta_n}{\theta_{n+a}} \text{ ——————— (111)}$$

The photographic traces over a wide range of initial amplitudes of the decaying oscillation were enlarged and the values of the decrement evaluated for small periods of time. The relationship of amplitude to damping was therefore obtained over the operating range of the instrument. A large number of points were tabulated and for the outer system, the dotted lines of Figure (18), show the limit of scatter of the experimentally obtained damping coefficients. A straight line could be drawn through the mean values of these results, giving an equation relating the non-dimensional damping coefficient to amplitude:-

$$d = 3.75\theta + 3.75 \times 10^{-4} \text{ ——————— (112)}$$

This relationship is in close agreement with similar tests carried out by numerous authors. Sumner and Entwistle (Reference 7) have graphs similar to figure (18) drawn for a mild steel specimen. Measurement of damping was, in their case, obtained by measuring the energy supplied to the system to maintain it in oscillation. The ratio of this energy to the total energy of the system per cycle is a measure of the damping capacity. At the

FIGURE 18

VARIATION OF DAMPING IN OUTER SYSTEM

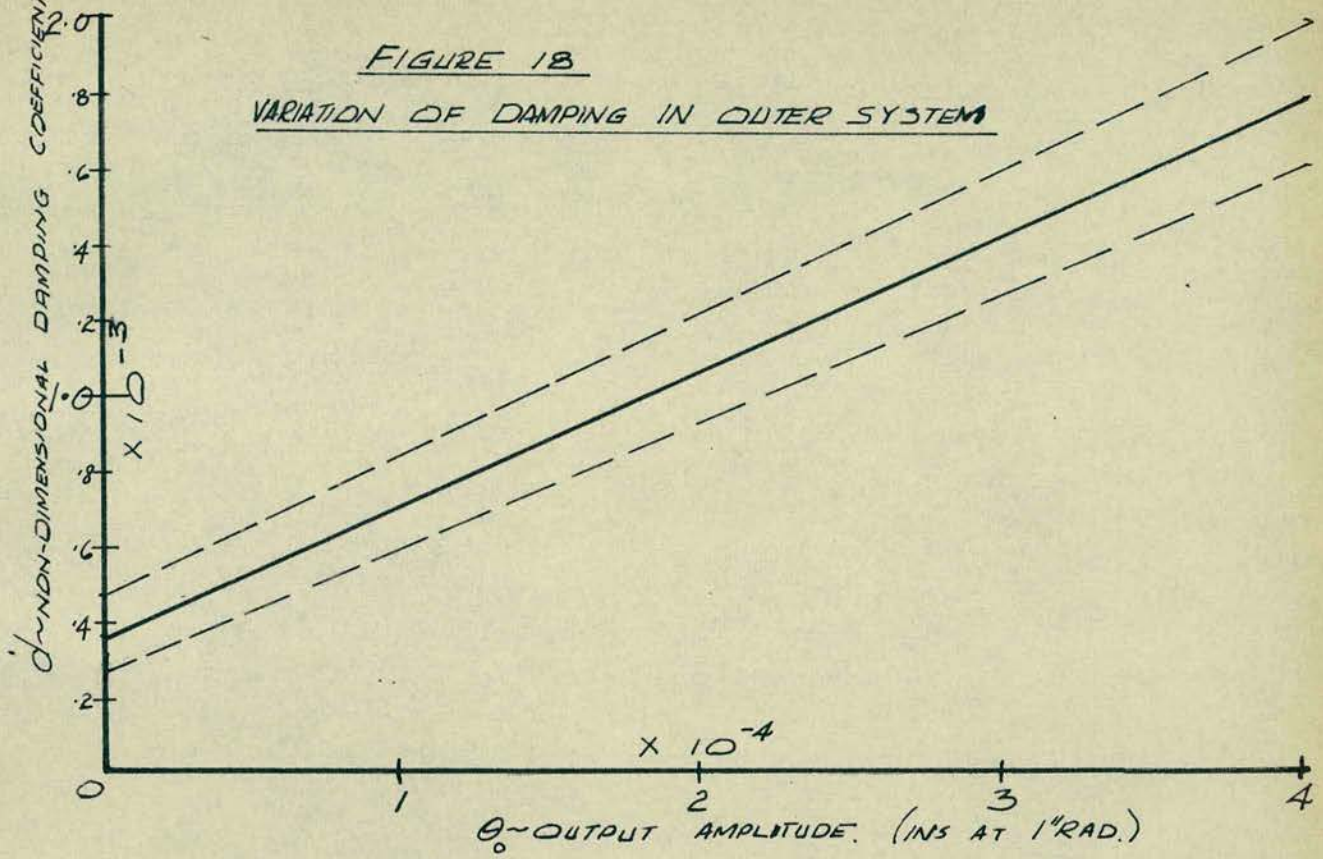

FIGURE 19

VARIATION OF DAMPING IN INNER SYSTEM.

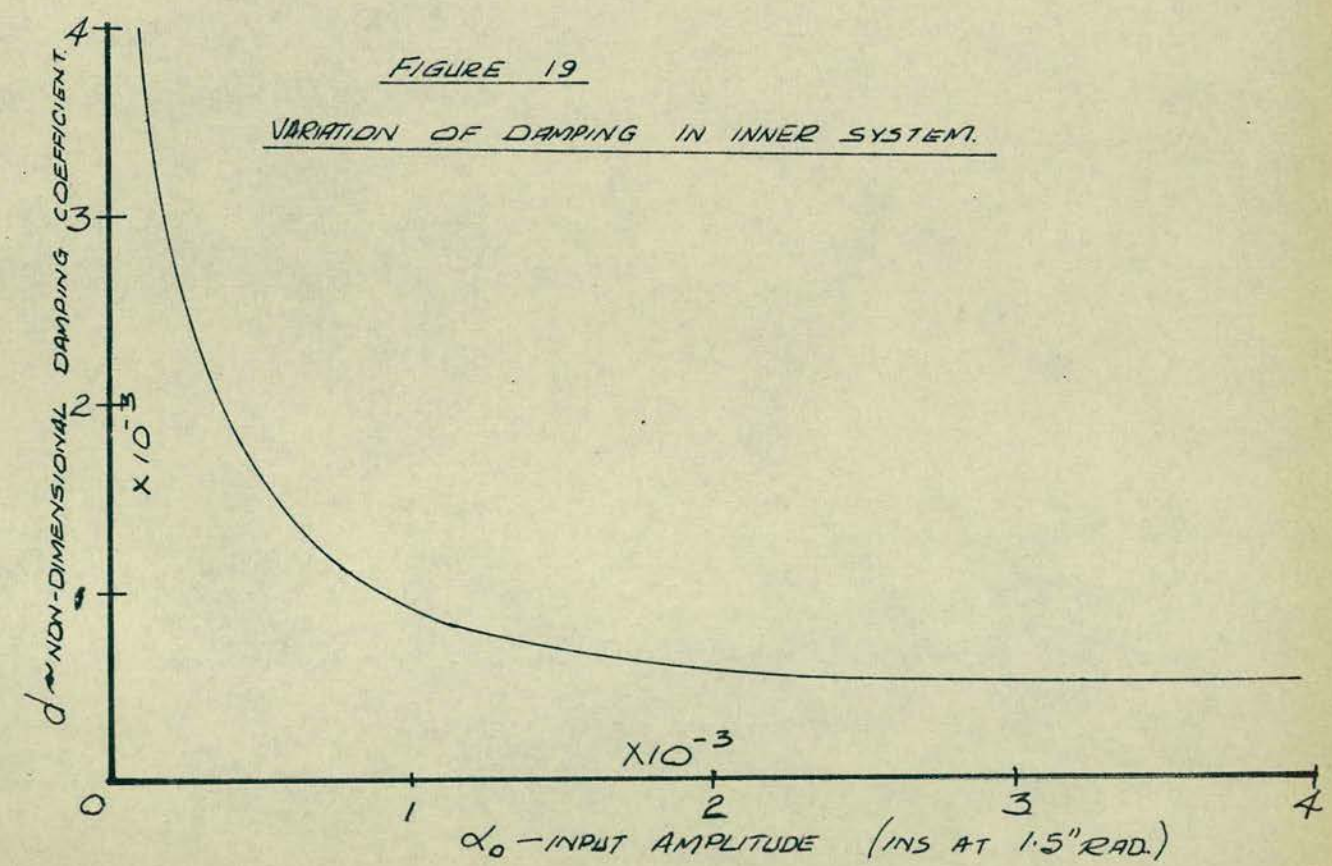

resonant condition the energy input per cycle to an oscillating system is $\pi C \omega_n \theta_0^2$ and the total energy equal to the maximum strain energy is $\frac{1}{2} k \theta_0^2$. The fractional energy loss can then be evaluated in terms of the logarithmic decrement used in the present damping tests, e.g.

$$\frac{\Delta E}{E} = \frac{\pi C \omega_n \theta_0^2}{\frac{1}{2} k \theta_0^2} = \frac{2\pi C}{A \omega_n} = \Delta \pi d = 2\delta \qquad \text{——— (113)}$$

Figure (18) and the results of Reference (7) for mild steel can be compared by the above relationship and for the range of stress encountered, the values are comparable. The slope of the latter is greater but this is to be expected, as the mild steel used in Sumner & Entwistle's tests was in the annealed condition, whereas, the present test instrument could be expected to have considerable internal stress due to machining operations.

Reference (7) also shows the effect of magnetizing the specimen and it can be seen that this reduces the damping capacity considerably. This reduction in damping can be visualized from the consideration of domain theory. In the demagnetized state, the ferromagnetic material has the preferred direction of its domains lying with a random distribution, making the resultant magnetization zero. During oscillation the movement of the domains due to

this random distribution, creates internal damping. In the magnetized, or 'domain alignment' state, the domains are held in alignment along the magnetic axis and thereby create less damping due to the reduction of internal friction.

Tests were carried out to establish the effect of magnetization on the present instrument. The procedure adopted was to pass a magnetic flux through the outer shafts by an electro-magnet, coupled to the supports of the instrument. The flux thereby passed through the outer shafts and gimbal, excitation by the systems electro-magnetic drive was not then effective. A mechanical vibration generator was applied to the frame, resonating at the resonant frequency of the outer system and the amplitude adjusted to lie within the normal operating range of the instrument. As in the previous tests, the damping coefficient was evaluated from the free vibration decay curve. The values of the damping coefficients obtained from this induced magnetism, as shown on figure (16), were considerably less than those obtained previously, although not as much a reduction as obtained by Sumner and Entwistle, primarily because of the difference in magnitude of the induced magnetization used in the two tests. The outstanding feature is that the damping, as well as being reduced, becomes much less

dependent on amplitude with a magnetized specimen.

The preceding damping analysis is concerned with the outer gimbal system only. Similar tests were carried out on the inner system before it was installed inside the gimbal and the non-dimensional damping factor was found to be within the region 0·0001. When the inner system was assembled inside the complete instrument it was found that the damping increased and its variation with amplitude was found to be different from that obtained with the outer system. In the inner system the damping, as can be seen from figure (9), decreased with increasing amplitude. This effect was due to electro-magnetic damping within the exciting system and was evident, because of the remnant magnetic flux, when there was no direct current flowing through the circuit.

5.2 Effect of Variation of Damping on Output

From the previous damping tests, it can be seen that the damping of both the outer and inner oscillating systems vary with the amplitude. With the inner rotor system maintained at a constant amplitude, only the variation of damping in the outer system need be considered as having an effect on the output of the system. This damping coefficient can be assumed to be proportional to the output from the

system. The equation of motion will therefore be amended by the replacement of the constant damping coefficient by the relationship $d = a\theta_0 + b$ where a and b have the numerical values of 3.75 and 3.75×10^{-4} for the present experimental set up.

i.e. $\ddot{\theta} + [2\omega_n (a\theta_0 + b)]\dot{\theta} + \omega_n^2 \theta = T\cos\omega t$ ——————— (114)

where $\omega_n = \sqrt{\frac{k_x}{A}}$ = undamped natural frequency

A = inertia of gimbal and rotor system about output axis

k_x = stiffness of gimbal and rotor system about output axis

T = torque due to rate of turn and unbalance

ω = forcing frequency.

This differential equation is, with the exception of the damping term, similar to equation (24) i.e. $2\omega_n(a\theta_0 + b)$ replaces $2\omega_n d$

Since the damping term remains constant for a given amplitude, equation (114) can be solved as the linear forced vibration equation to give the steady state solution:-

$$\theta = \frac{T\cos(\omega t - \psi)}{A\omega_n^2\sqrt{(1-f^2)^2 + [2f(a\theta_0 + b)]^2}} \qquad \text{——— (119)}$$

where $\psi = \tan^{-1}\left[\frac{2f(a\theta_0 + b)}{1 - f^2}\right]$

or $$\theta_0 = \frac{T}{A\omega_n^2\sqrt{(1-f^2)^2 + [2f(a\theta_0 + b)]^2}} \qquad \text{——— (120)}$$

To obtain an explicit solution for θ_0 both sides of equation (120) must be squared and rearranged to give:-

$$(2a)^2\theta_0^4 + 8ab\theta_0^3 + \left[(2b)^2 + \left(\frac{1-f^2}{f}\right)^2\right]\theta_0^2 = \left(\frac{T}{A\omega_n^2 f}\right)^2 \qquad \text{——— (121)}$$

(PAGE 60 HAS BEEN OMITTED.)

By substituting $\phi = \theta_0 \times 10^4$ and the values of a and b found from the damping tests (i.e. a = 3.75, b = 3.75 x 10^{-4}), equation (121) can be simplified for the balanced system to:-

$$\phi^4 + 2\phi^3 + \left[1 + \left(\frac{1-f^2}{7.5\times10^{-4}f}\right)^2\right]\phi^2 - 0.45\,\Omega^2 = 0 \qquad \text{——— (122)}$$

In the unbalanced system, the in-phase unbalanced effects can be neglected as they merely shift the intersection of the output and rate of turn axes. The term $\left[\Omega^2 + (\omega\epsilon)^2\right]$ can then be substituted for Ω^2 in equation (122) to give, as an equivalent axis tilt, the equation for an unbalanced system. From Chapter 4.6 (equation 107), it can be seen that with unbalance present in the system, the frequency ratio f can be related to the unbalance in the system,

i.e. $f = 1 - 0.266\epsilon$

By substituting in equation (122), an equation relating output to unbalance and rate of turn can be obtained, i.e.:-

$$\phi^4 + 2\phi^3 + \left[1 + \frac{10^8}{7.5^2}\left(\frac{2\epsilon - \frac{\epsilon^2}{3.76}}{3.76-\epsilon}\right)^2\right]\phi^2 - 0.45\left[\Omega^2 + \left\{\omega_n\epsilon\left(1-\frac{\epsilon}{3.76}\right)\right\}^2\right] \qquad \text{——— (123)}$$

For small values of unbalance, i.e. $\epsilon \ll 1$ this equation can, for the parameters of the present experimental instrument, be reduced to:-

$$\phi^4 + 2\phi^3 + \left[1 + 0.5(\epsilon\times10^3)^2\right]\phi^2 - (\alpha_0\times10^3)^2\left[12.5(\epsilon\times10^3)^2 + 1.44\Omega^2\right] \qquad \text{——— (124)}$$

This is a fourth order equation of the form:-

$$\phi^4 + a_3\phi^3 + a_2\phi^2 - a_0 = 0$$

The first derivative of this equation shows that a change of slope occurs at the value $\phi = 0$. The second derivative shows that this is a minimum value provided a_3, a_2 and a_0 are positive. As ϕ approaches $+\infty$ the equation becomes positive, illustrating that there must be at least one positive root to the equation. Descartes Rule establishes that there is only one such positive real root to equation (124).

Figure (20) shows the effect of the damping variation on output, the bending over of the response with increasing θ becomes more pronounced as the rotor amplitude increases. A point is reached when any increase in the input to the system merely compensates for the increase in damping and there is consequently no increase in output.

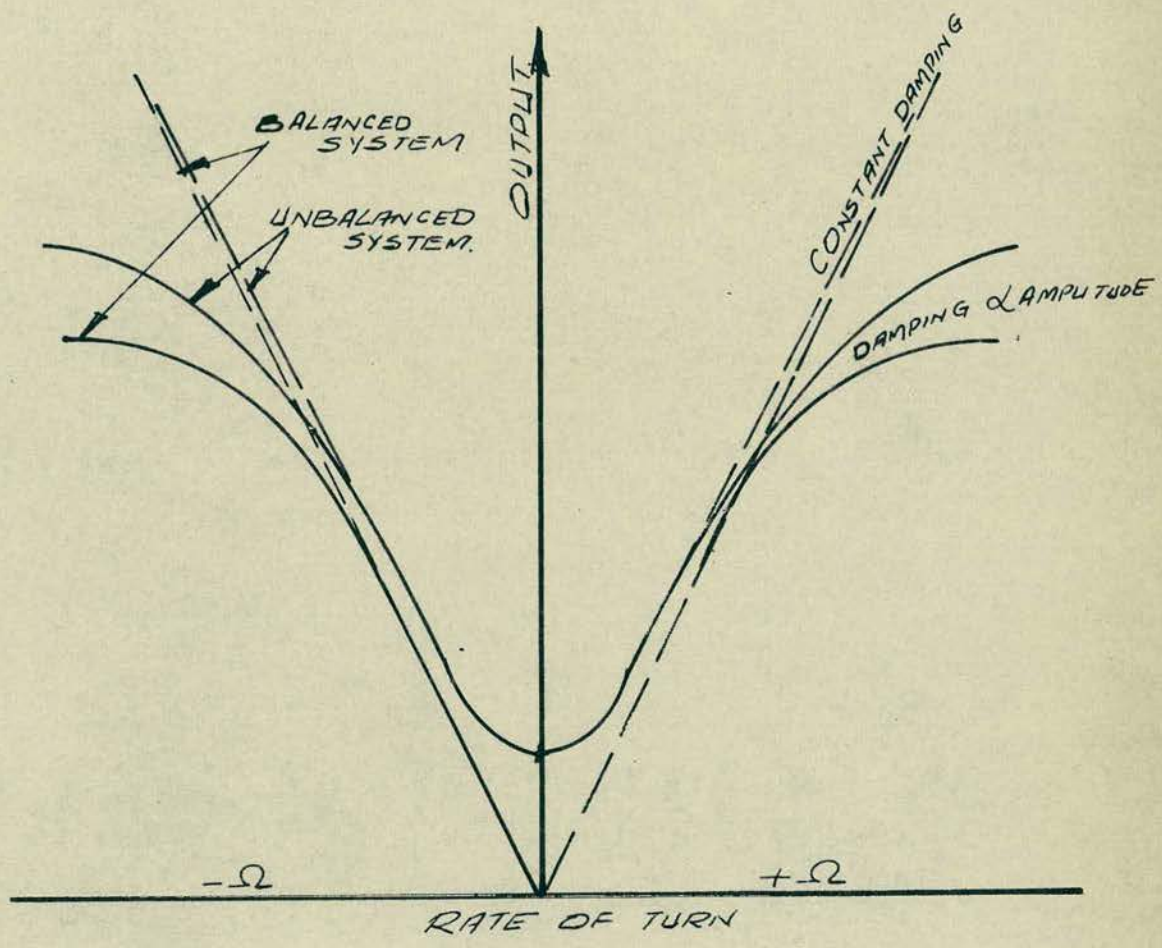

FIGURE 20

EFFECT OF DAMPING ON OUTPUT.

CHAPTER 6

6.0 Frequency Selection and Sensitivity of the Instrument

6.1 Frequency Selection

It can be seen from Chapter 4.5 that the output from the system, due to the principal forms of unbalance, is proportional to the inertia forces and is therefore a function of the acceleration of the system. The output, due to an applied input signal, is proportional to the Coriolis forces and depends upon the velocity of the system. The combined output from these two sources can be expressed as:-

$$\theta_o = DM\left(\sqrt{(C_1\Omega\ddot{\alpha})^2+(C_1\epsilon\ddot{\alpha})^2}\right) \qquad (125)$$

where DM is the dynamic magnifier of the system and depends upon the frequency ratio and damping coefficient of the system, C_1 is the inertia of the rotor about the rotor axis. $\dot{\alpha}$ and $\ddot{\alpha}$ represent the velocity and acceleration respectively, of the rotor about its axis. Ω is the applied rate of turn applied about the input axis and ϵ represents the resultant unbalance expressed in terms of axis tilt.

With $\alpha = \alpha_o \sin\omega t$ equation (125) can be rearranged to give:-

$$\theta_o = DM.\ C_1\ \omega\ \alpha_o\left(\sqrt{\Omega^2+(\omega\epsilon)^2}\right) \qquad (126)$$

This equation shows that the combined output is proportional to $\left[\Omega^2+(\omega\epsilon)^2\right]^{\frac{1}{2}}$ and the proportion of this

attributed to the input signal reduces as the operating frequency ω is increased. To minimize the effects of unbalance, it is therefore desirable to use a low operating frequency.

For a system containing no unbalance and using displacement type pick-ups, it can be shown that to obtain a gain in output, an increase in frequency is not justified. To determine the output available from various design parameters a 3" diameter by 1" thick rotor with rotor shafts $\frac{3}{8}$" diameter and $\frac{3}{4}$" long was used as the basis of comparison. This gives a torsional natural frequency of approximately 500 cps and an output proportional to $(\alpha\omega)$. The ratio of the output obtained with this design to that obtained with any of the parameters permissable from figure (22) is plotted in figure (21). This diagram shows that, for an instrument of reasonable dimensions, an increase in frequency by a factor of 10, merely gives a gain of 5, in output amplitude. The diameter and length have to be increased considerably to attain this higher frequency, giving a much more cumbersome instrument.

Measurement of the output by accelerometer rather than by displacement gauges does not give a greater output within the range 0 - 600 cps. At higher frequencies an increase in response is obtained

FIGURE 21.

GAIN OVER PRESENT SYSTEM BY INCREASING NAT^{L} FREQUENCY.

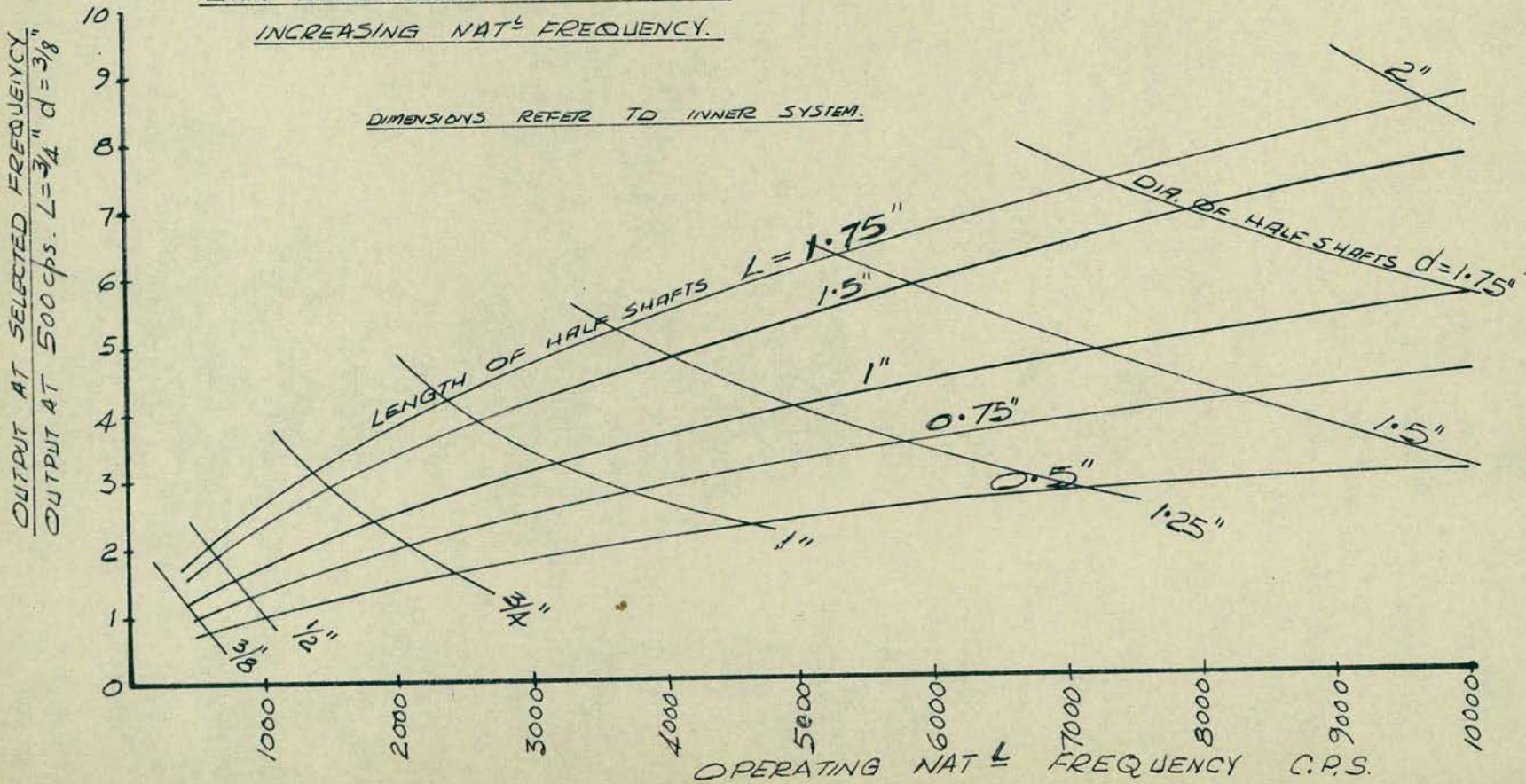

by accelerometers but this is offset by the disadvantage that an accelerometer requires a mass built into, or in close contact with, the instrument. The proximity type displacement gauge, used in the experimental work, does not have this disadvantage.

As can be seen in Chapter 3.3, the inoperative time of the instrument, which occurs due to the transient condition when the input rate of turn is changed, is inversely proportional to the operating frequency. The requirement to operate at a low frequency does not therefore reduce this inoperative time and provision to reduce this by an alternative method will be required.

6.2 Sensitivity of the Instrument

In a completely balanced system the output, due to a constant input signal Ω is, from Chapter 3.1, equal to:-

$$\theta_o = \frac{-\alpha_o f C_1 \Omega \cos(\omega t - \phi)}{A\omega_n \sqrt{(1-f^2)^2 + (2df)^2}} \qquad (126)$$

Assume that for this balanced system, the frequency ratio f is equal to unity. The amplitude of the output is then:-

$$\theta_o = \frac{-\alpha_o C_1 \Omega}{2A\omega_n d} \qquad (127)$$

$$= \frac{-\alpha_o C_1 \Omega}{C_x} \qquad (128)$$

The sensitivity of the balanced instrument

will depend upon the variables of equation (128). To enable small rate of turn signals to be detected, the rotor amplitude α_0 and the inertia of the rotor C, must be as large as possible. The damping must be low and instrumentation capable of detecting small output oscillations will be required. In the present experimental instrument, a value of 0.02 lb.in.sec. has been achieved for the damping coefficient. It has also been shown that this value can be reduced by passing a magnetic flux through the instrument. Reference (7) shows that this magnetism can reduce the damping coefficient to approximately 0.0005 lb.in.sec. with little variation over the stress range. With a rotor inertia similar to that used in the present experimental instrument (i.e. 60×10^{-4} lb.in.sec.^{2}) a completely balanced, idealized instrument could, theoretically, be capable of recording rates of turn as small as earths rate. This would require a rotor amplitude of the order of ·001 Radian and instrumentation capable of measuring oscillations as small as 10^{-6} ins. The present instrument gives an output of approximately 600 mV per 10^{-3} inch deflection, therefore, with small modifications, it should be capable of detecting oscillations as small as the earths rate.

To record small rates of turn, the unbalance

in the system would either have to be eliminated ~~or neglected~~ by instrumentation. Chapter 4.5 shows that by neglecting in-phase unbalance signals, the output signal can be considered proportional to $\sqrt{(C,\Omega)^2 + (C,\omega\epsilon)^2}$ where $C,\omega\epsilon$ represents the resultant unbalance expressed as an axis tilt. To record inputs as small as earths rate, the proportion of the signal due to unbalance must be less than this input.

$$\left.\begin{array}{ll} \text{i.e.} & \Omega > \omega\epsilon \\ \text{or} & \epsilon < \frac{\Omega}{\omega} \end{array}\right\} \quad -- (129)$$

Equation (129) shows that to record earths rate with the forcing frequency of 500 cps used in the present instrument, the unbalance must be reduced to less than 2.4×10^{-8} Radians. By reducing the frequency, this tolerance could be increased.

As discussed in Chapter 4.0, a phase sensitive voltmeter could, due to differences in phase, differentiate between rate of turn and the principal unbalance effects. Perhaps by this method and by adding a small unbalanced mass, in close proximity to the top of the rotor, and displaced by a small distance from the OY axis (i.e. $\beta \rightarrow 90^\circ$ and $b \rightarrow 0$), low input rate of turn signals can be recorded.

A further limitation would, however, be the stability of the oscillator, as this would have to be

controlled in frequency to within approximately 5 parts per million for a damping coefficient of 0·002 lb.in.sec. This stability would be required to ensure that the drop in output, due to the drift from resonance, did not exceed 10%.

The present experimental instrument is capable of measuring only high rates of turn of the order of 1·0 rpm. This is principally due to the magnitude of unbalance and type of excitation used. Also the sensitivity was greatly reduced by the uncertainty of the tuning of the instrument, which occurred when a mass was added,or when an attached mass shifted,due to the oscillation of the rotor.

Greater sensitivity could also be obtained through reducing the damping by magnetization of the output shafts. This was observed, but due to the difficulty in mounting the electro-magnet across the output shafts, this procedure was not used in subsequent tests.

CHAPTER 7

7.0 Instrument Design

Figure (1) shows the configuration of the instrument. The rotor, which is fixed to the outer gimbal, is set in torsional oscillation about the rotor shafts. With a rate of turn applied about the input axis, Coriolis forces are set up, which oscillate the gimbal about the output shafts. These output shafts are held by end supports which are bolted to the baseplate of the instrument.

7.1 Inner System

From the differential equation of motion of the system, it can be seen that the output from the system is proportional to the torque induced by the Coriolis acceleration. This torque is numerically equal to the product of the angular momentum about the rotor axis and the rate of turn applied about the input axis.

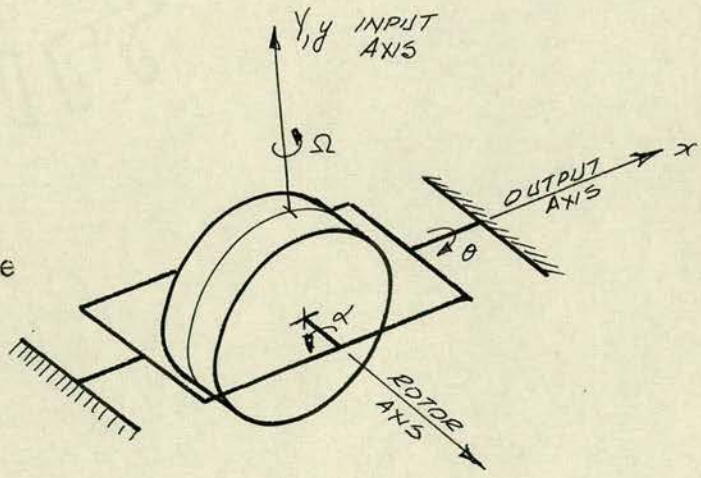

i.e. Torque about the output shafts, $T_x = C_1 \dot{\alpha} \Omega$ ——— (130)

where C_1 = Inertia of the rotor about the oz-axis

$\dot{\alpha}$ = Velocity of the rotor about the oz-axis

Ω = Rate of turn applied about the input axis

with $\alpha = \alpha_0 \sin \omega t$ equation (130) becomes:-

$$T_x = C_1 \alpha_0 \omega \Omega \cos \omega t \qquad (131)$$

It can be seen that for maximum output and sensitivity from the instrument, this torque must be a maximum, the limiting case being the stress in the input shafts. This stress can be evaluated from the characteristic equation:-

$$\frac{T}{J} = \frac{G\theta}{L} = \frac{2\tau}{d} \qquad (132)$$

where T = Torque applied to shafts lb/ins.

J = Polar moment of inertia of shaft $in.^4$

G = Modulus of Rigidity $lb/in.^2$

θ = Angular displacement of rotor Rad.

L = Length of Shafts ins.

τ = Shear stress at diameter d $lb/in.^2$

d = Diameter at which stress is considered ins.

giving $\tau = \frac{G\theta d}{2L}$ ——— (133)

The torsional natural frequency of the inner system can be found from:-

$$\omega_n^2 = K/C_1$$

where ω_n is the torsional natural frequency

K is the stiffness of the rotor shafts = T/θ

Substitute for the stiffness coefficient in this frequency equation to obtain:-

$$\omega_n^2 = \frac{GJ}{L_{eq} C_1} \qquad \text{——————} (134)$$

where L_{eq} is the equivalent shaft length, equal to $L/2$ for two shafts connected to either side of the rotor and L is the length of the individual shafts.

$$\therefore \omega_n^2 = 0.197 \frac{Gd^4}{C_1 L} \qquad \text{——————} (135)$$

The natural frequency considered is the undamped natural frequency which, for the small damping factors encountered in this instrument, can be considered to be numerically equal to the damped natural frequency of the system.

To obtain suitable practical values, a rotor of convenient dimensions can be used as the starting point. In the present analysis it was decided to commence with a rotor of 3" diameter by 1" thick, giving for mild steel, an inertia of 58.1×10^{-4} lb.in.sec.^{2} about the o_3-axis. From this starting point, using equations (133) and (135) graphs of the relationship between the amplitude for a given stress and natural frequency were plotted in figure (22) for the common parameters d and L. The deflection δ is measured at a radius of 1".

A further limitation must be imposed to

FIGURE 22

GRAPH OF FREQUENCY & AMPLITUDE AGAINST LENGTH & DIA. OF HALF SHAFTS

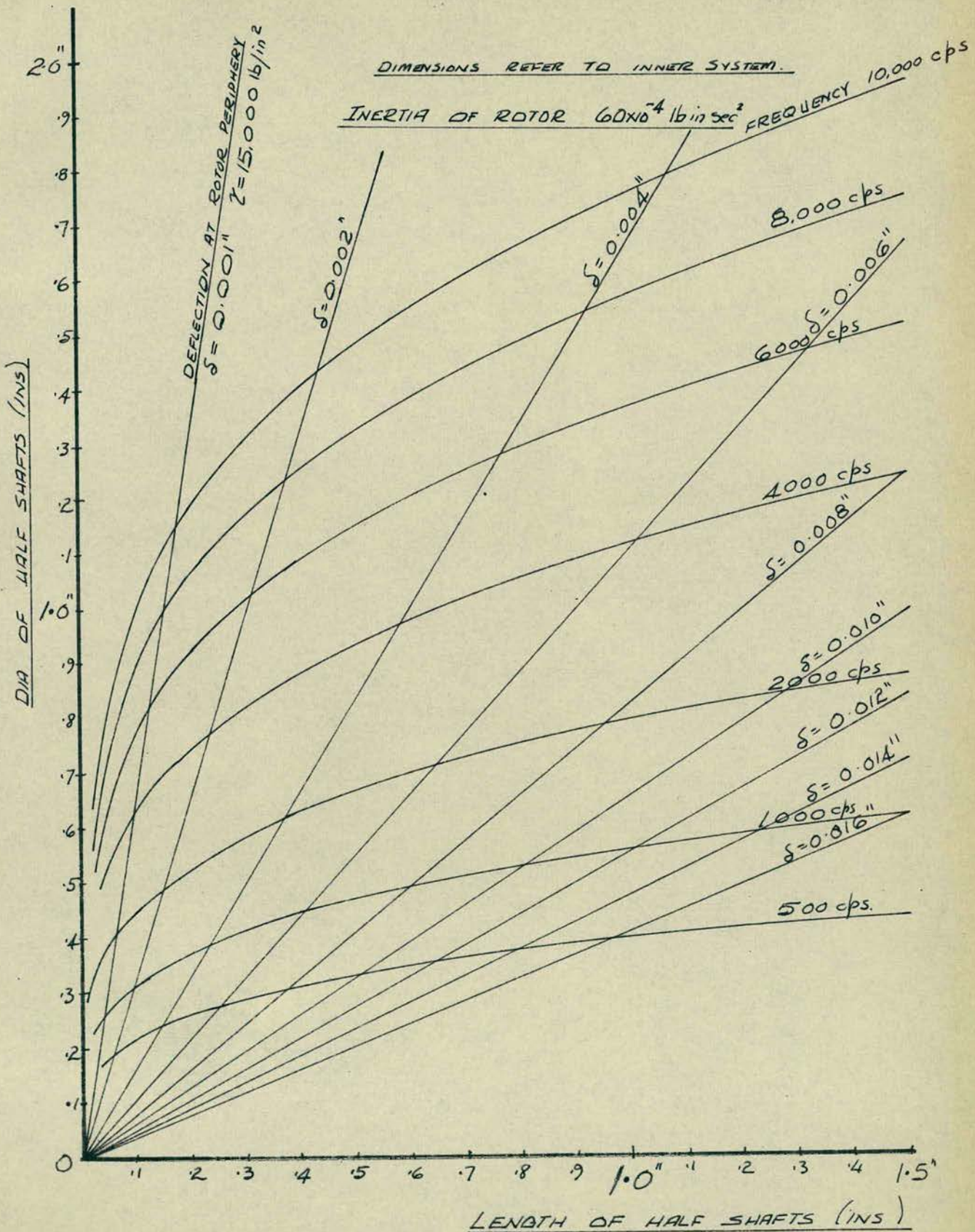

ensure that a bending natural frequency ω_B does not appear within the range chosen from figure (22) for the torsional natural frequency,

$$\text{i.e. } \omega_B = \chi\, \omega_n \qquad \text{——————} \quad (136)$$

where χ is a factor introduced to ensure the elimination of ω_B the bending natural frequency from the operating torsional range. The bending natural frequency is, as a first approximation, evaluated considering the end supports to be simply supported. This would be the case with abutments as small as the gimbals in a practical instrument.

$$\text{i.e. } \omega_B^2 = \frac{K}{M} = \frac{Kg}{W} \qquad \text{——————} \quad (137)$$

Assume that the rotor itself does not deflect and that all the static deflection Δ takes place in the rotor shafts,

$$\left.\begin{array}{l}\text{i.e. static deflection of the rotor} \\ \text{relative to the gimbal}\end{array}\right\} = \Delta = \frac{WL^3}{6EI} = \frac{W}{K} \quad (138)$$

where W is the weight of the rotor, and L, E, I and K are the length, Youngs Modulus, Moment of Inertia in bending and Stiffness, respectively, for the rotor shafts.

$$\therefore \omega_B^2 = \frac{6EIg}{WL^3} \qquad \text{——————} \quad (139)$$

$$\text{or } \omega_B^2 = \frac{114Ed^4}{WL^3} \qquad \text{——————} \quad (140)$$

Substitute for equations (135) and (140) into equation (136) to give:-

$$\frac{114Ed^4}{WL^3} = \chi^2\left(\frac{0.197Gd^4}{C_1L}\right) \qquad \text{——————} \quad (141)$$

By using a shaft material which has Poisson's Ratio

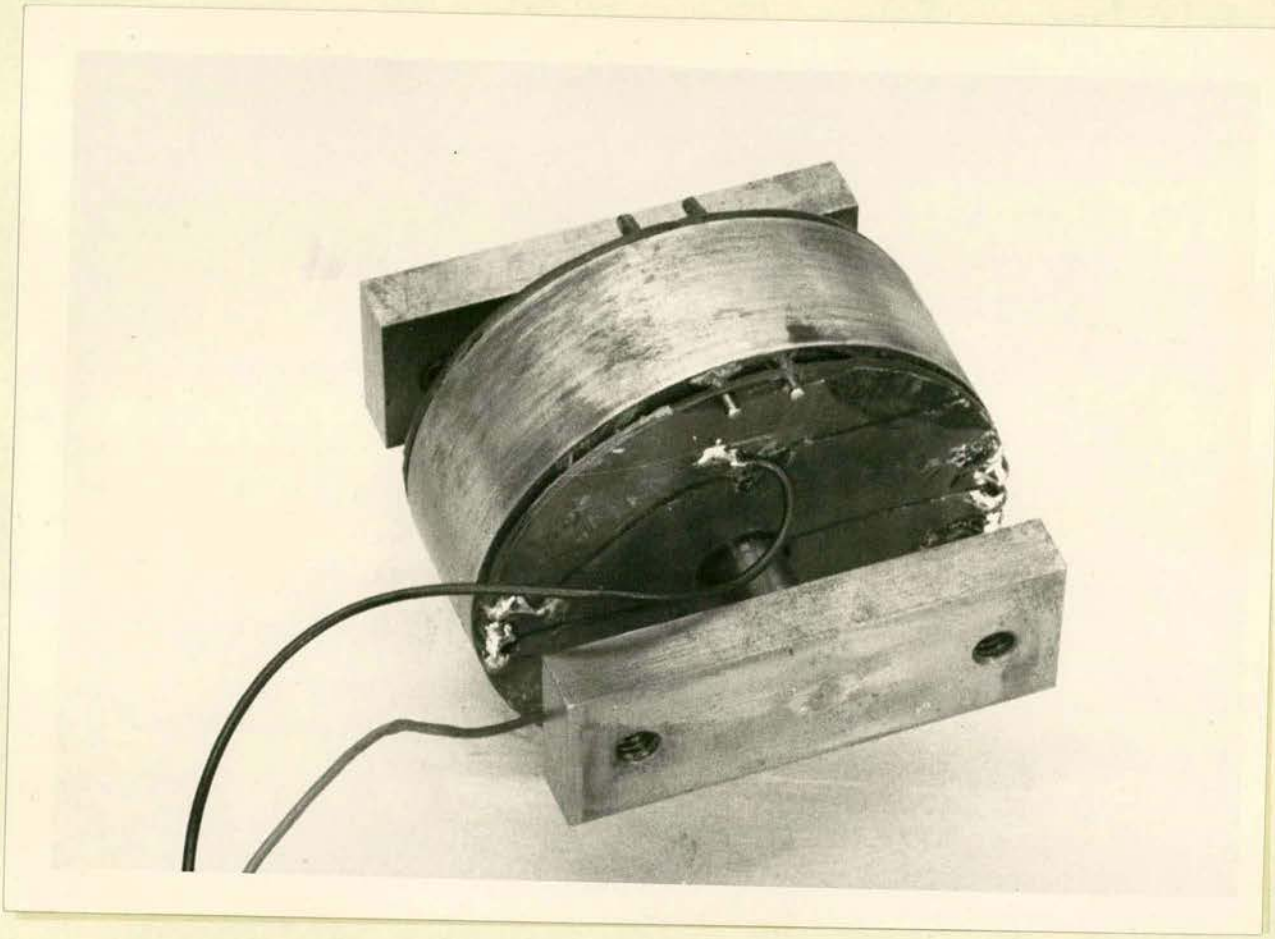

FIG. 23 INNER ROTOR SYSTEM.

equal to 0.25, Youngs Modulus E can be assumed to be equal to 2.5 times the Modulus of Rigidity G,

i.e. $E = 2.5\ G$

On rearrangement, equation (141) becomes:-

$$\frac{C_1}{WL^2} = X^2\ 6.9\times10^{-4} \qquad (142)$$

For a solid rotor $C_1 = \frac{WD^2}{8g}$

where D = diameter of rotor

hence $$\frac{D}{L} = 1.46X \qquad (143)$$

This equation can be used as an approximate check on the separation of the two natural frequencies. In the optimum case, with the shafts considered simply supported, the torsional frequency would be designed to be lower than the bending natural frequency, i.e. $x>1$. This would ensure that any building in effect imposed by the end supports, which increases the bending natural frequency, would carry this frequency further away from the range of the operating torsional frequency. With a 3" diameter rotor and $X \leq 1.2$ (i.e. 20% separation between ω_n and ω_B), equation(143) determines that shaft lengths in excess of 1.7" should be neglected.

After deciding upon a rotor inertia, graphs similar to figure (22) can be plotted from equations (133) and (135). These graphs, together with the requirements of equation (132) determine the frequency and amplitude available for any given

stress, enabling a first approximation to be made for a suitable design.

7.2 Outer System

The design of the outer system depends upon the overall dimensions previously chosen for the inner system. After a design for this has been established, a gimbal of a suitable size can be arranged to accommodate this inner system. The inertia of the gimbal and its torsional natural frequency are therefore fixed by the choice of the parameters of the outer system, leaving only the dimensions of the output shafts to be determined.

By substituting the inertia of the gimbal system about the output axis in place of the rotor axis in equations (133), (135) and (142), suitable dimensions for the output shafts can be obtained. Equation (142) considers that the mass is a rigid structure and that all the deflection takes place in the shafts. This may not be the case in the outer system as the deflection of the gimbal itself would have to be included. However, since equation (142) is considered only as a first approximation, this gimbal deflection can be neglected in the preliminary stages.

The tuning of the resonant frequency of the outer system to that of the inner system can be

achieved by mounting small tuning screws on the face of the gimbal figure (24). By extending these tuning screws the inertia of the gimbal system is increased, with a consequent lowering of the torsional frequency, while the bending frequency remains unchanged.

In the event of a bending natural frequency of the system coinciding with the torsional frequency, the shaft lengths can be extended slightly to give the necessary frequency separation, as the torsional and bending natural frequencies are inversely proportional to the shaft length and shaft length cubed respectively.

7.3 Experimental Instrument

The instrument used throughout the experimental work was constructed from material readily available and sizes convenient for machining purposes. The inner system, as shown in figure (23) consists of a 3" diameter by 1" thick mild steel rotor, with shafts $\frac{3}{8}$" diameter and $\frac{3}{4}$" long, integral with a section of the gimbal. The effective inertia of the rotor about the rotor axis was therefore 58.1×10^{-4} lb.in.sec.^{2}, with torsional and bending natural frequencies of 470 and 1400 cps respectively. These parameters give from (figure 22), a deflection at the rotor periphery of $\pm$ 0.008 in. with a shaft

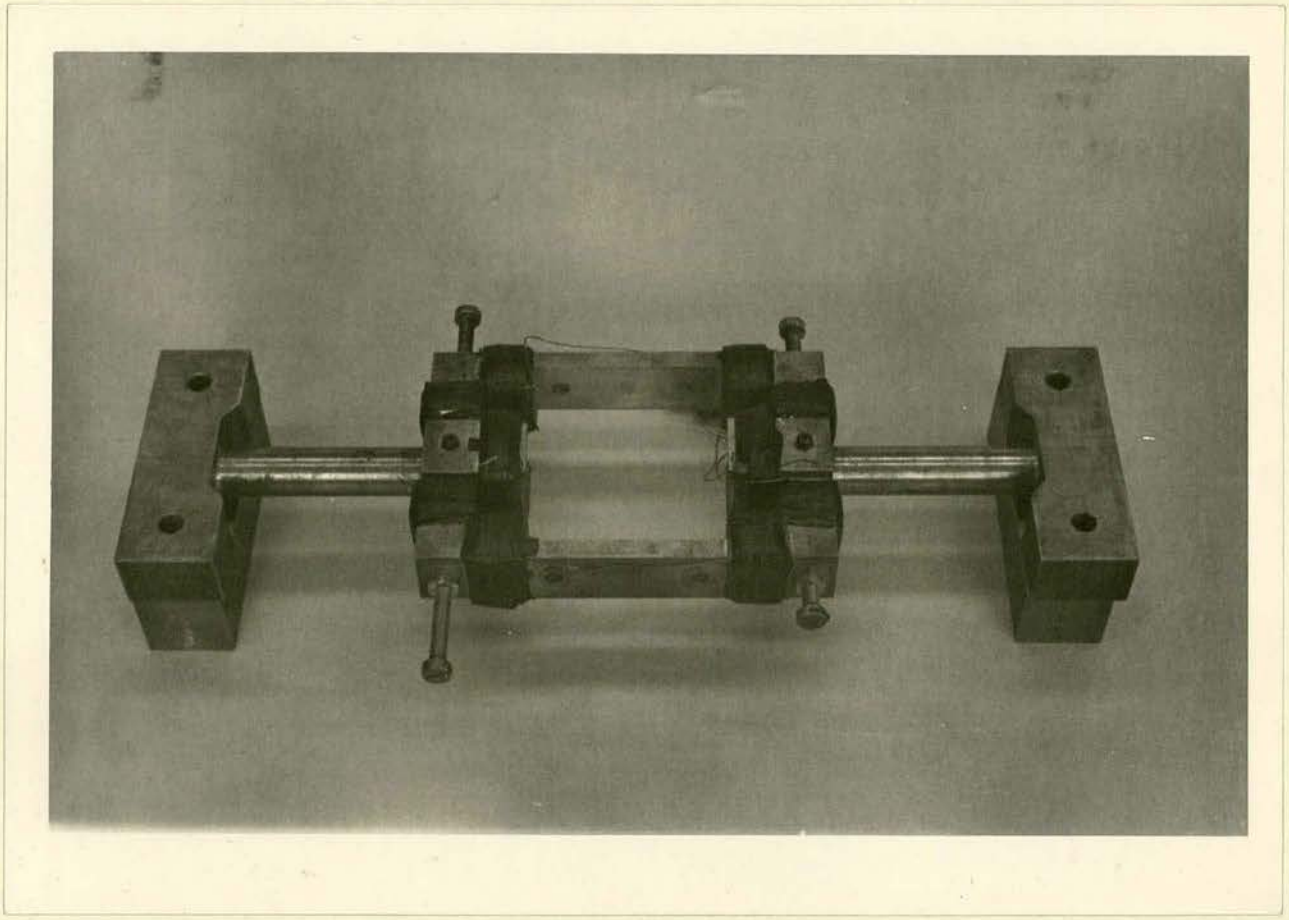

FIG. 24 OUTER GIMBAL SYSTEM.

stress of 15,000 lb/in^2.

An outer system having sufficiently rigid gimbals and yet maintaining a reasonably light structure was constructed, as shown in figure (24). This gave an inertia of the gimbal and rotor about the output axis of 2.2×10^{-2} lb.in.sec^2. With a gimbal thickness of 1 in., it was decided to have the output shafts $2\frac{3}{4}$ in. long by 0.68 in. diameter thereby giving the torsional natural frequency of 470 cps. The outer or gimbal system was machined from a solid piece of mild steel and then mounted, by brass distance pieces and brass bolts, to the base-plate of the instrument. The distance pieces and bolts were required to be constructed of brass due to the type of exciting system used. The outer gimbal was recessed to receive the rotor system, final fixing being achieved by four $\frac{1}{4}$" diameter machine screws and nuts. The fundamental bending natural frequency of the outer system, with the complete instrument bolted to a test bed, was found experimentally to be 350 cps., which is approximately the same as the value calculated with the end supports pinned. When the instrument was later mounted on rubber, to eliminate vibration transmitted by the rough running of the rate of turn table, the fundamental bending frequency rose to 440 cps. This

was considered to be undesirably near the operating torsional frequency. Since the calculated value of the bending frequency, when considering the end supports to be built-in, was 750 cps, it was decided to modify the bolting down arrangement to bring this bending frequency close to the built-in condition. A heavier baseplate was installed in an attempt to achieve this condition. This, together with various additional clamping arrangements of the end supports, merely lifted the bending frequency to 480 cps., which was even closer to the torsional frequency than before. As discussed previously, it was then decided to alter the bending frequency by increasing the length of the shaft. The shafts were increased to 3 in. and to retain the former torsional frequency, a small amount was machined from the outer side of the gimbal. The nett effect was to obtain torsional and bending frequencies of 470 and 386 cps respectively. The final tuning of the torsional frequency to that of the inner system was provided by the tuning screws.

7.4 Exciting System

The type of excitation used in the present instrument is of the electro-magnetic type. A magnetic flux was induced to flow between two pole pieces attached to the gimbals at a point adjacent to

the rotor. The gap between the rotor and pole pieces was 0.006 in. Conductors were inserted at the periphery of the rotor to cut the lines of magnetic flux so that when an A.C. currentwas applied to the conductors, torsional oscillation of the 'rotor' was achieved. Three of these conductors, constructed of 14 swg., were inserted in the rotor periphery adjacent to each pole piece. The conductors were connected in series by means of printed circuits attached to the face of the rotor (Figure 23). External leads were then led out of the instrument, through an impedance matching transformer, to the oscillator.

It was initially anticipated that the necessary flux could be achieved by the remnant flux obtained after magnetization of the gimbals by means of coils This did not produce the desired effect and was probably due to the large leakage and eddy current effects as the rotor and gimbals were of solid, rather than laminated, construction. The coils, of 24 swg, were then rewound and an equivalent mass machinedfrom the gimbals to compensate for the inertia of these coils. A direct current was then applied to the external leads from these coils to obtain a suitable magnetic flux. The coils produced a major

disadvantage in that the power dissipated in the form of heat, raised the temperature of the complete instrument considerably so that the damping and other characteristics of the system were changed. This resulted in reducing the output for a given input signal to 20% of the original signal within a period of thirty minutes. (figure (25). To overcome this effect, it was decided to limit the direct current and therefore the rotor amplitude to values which do not raise the temperature of the gimbal above a steady state temperature.

It is felt that this type of excitation could be improved upon to give greater output and good stabilization. An improvement to the existing arrangement would be to wind the coils external to the gimbal, thereby passing the flux in at one support of the instrument and out at the other support. This would also improve the damping characteristics as discussed in Chapter 5. The gimbal would have to be modified with brass inserts. to prevent flux passing along the gimbal instead of across the rotor gap.

FIGURE 25

DECAY OF OUTPUT DUE TO HEATING

ROTOR AMPLITUDE ~ 2×10^{-3} INS AT 1½" RAD.

RATE OF TURN. ~ 10 RADS/SEC. (CONSTANT.)

POWER INPUT. ~ DC 1·99A 16V
AC 5V

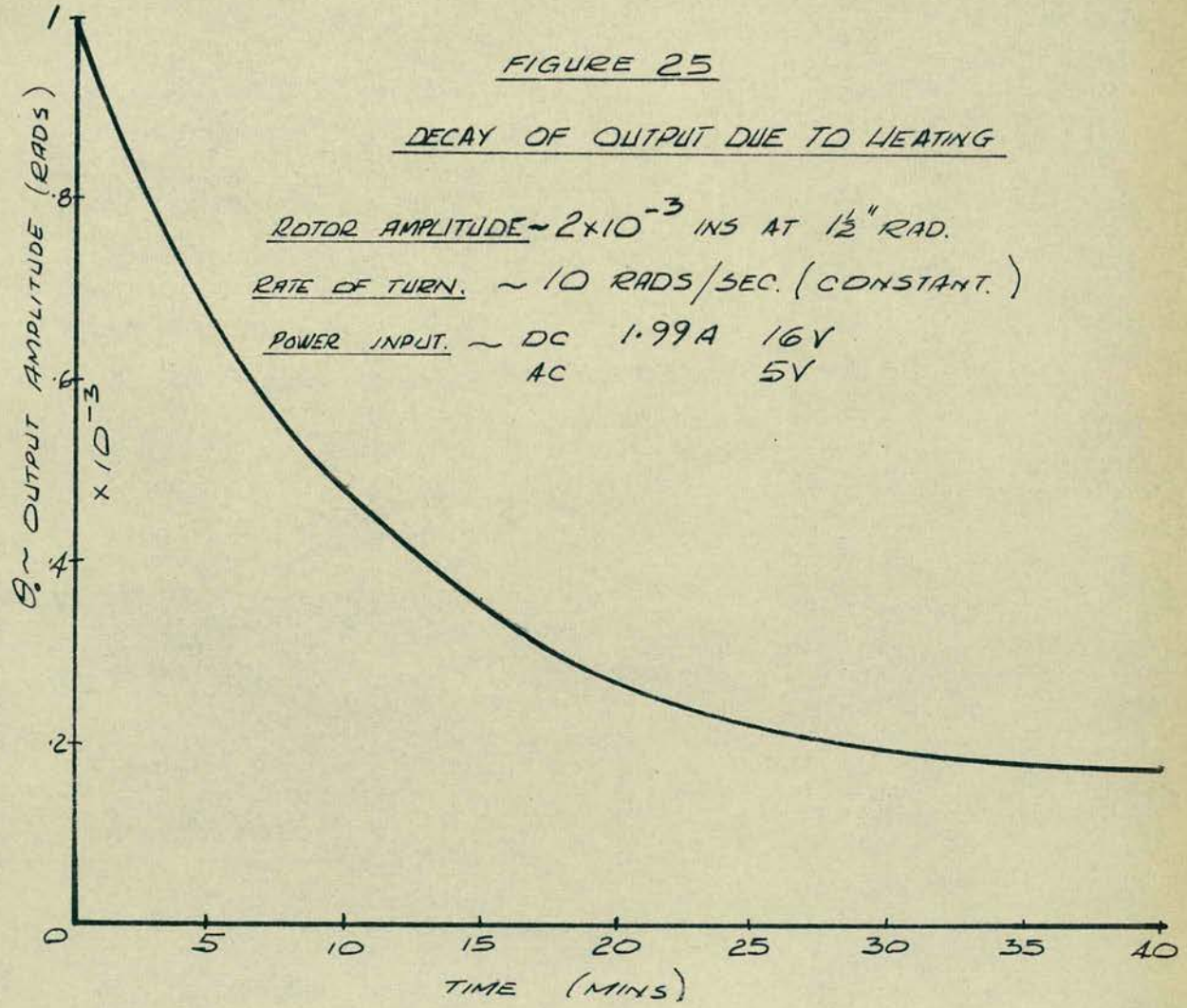

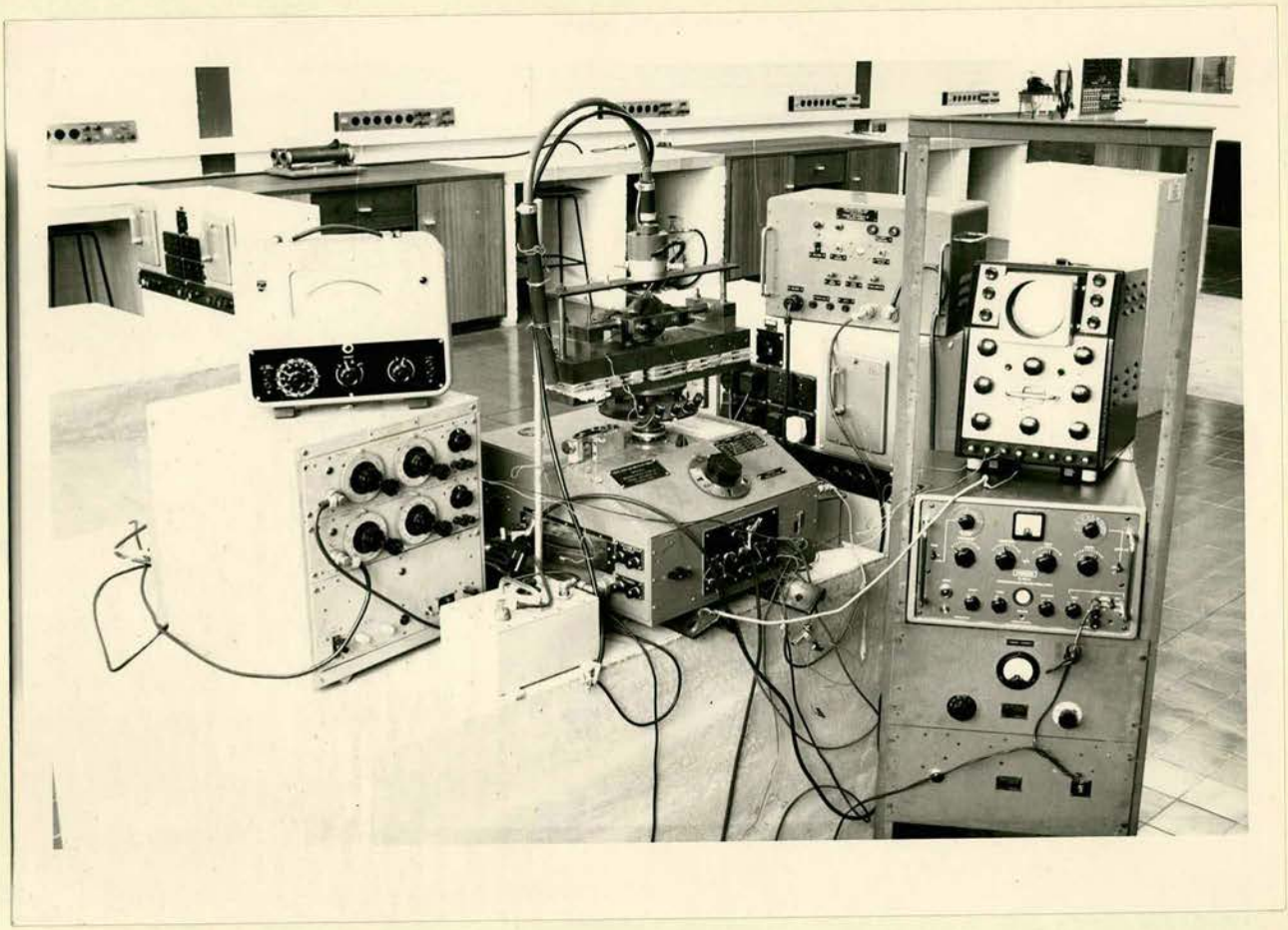

FIG 26 APPARATUS.

CHAPTER 8

8.0 Apparatus and Instrumentation

As discussed in Chapter 7, the excitation of the rotor depends upon a direct current being supplied to the magnetic circuit and an alternating current being supplied to the conductors. The individual components used to produce these two supplies together with the instrumentation as shown in figure 26 are summarized in the following paragraphs.

8.1 Direct Current Supply

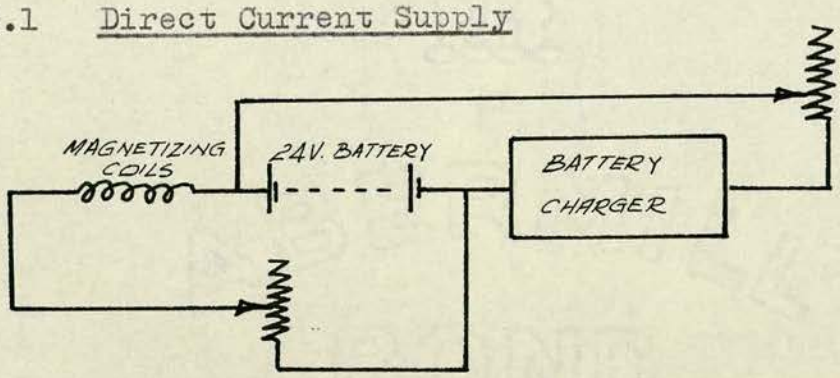

FIG 27.

Figure 27 shows a diagrammatic arrangement of the d.c. supply to the magnetizing coils which are wound in series around the gimbal. The power is supplied by two, twelve volt lead-acid batteries.

To ensure an even supply of current to the coils, a battery charger was coupled to the battery to maintain it at a constant level of charge. Resistances were installed enabling the load to the coils, and the charge to the battery to be varied.

8.2 Alternating Current Supply

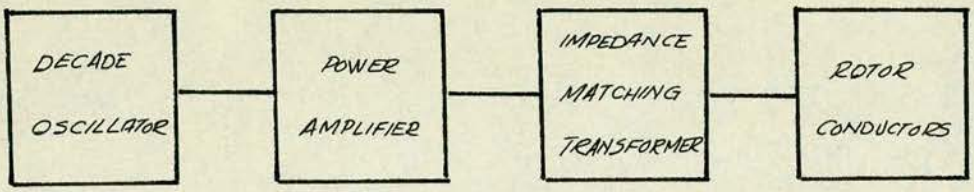

FIG 28

Figure 28 shows a block diagram of the components used to give the alternating, excitation current to the rotor conductors.

Initially, the signal was generated by a Goodmans type D5 power oscillator, but this had to be replaced by an instrument having better selectivity and stability. A Muirhead Decade Oscillator coupled to a power amplifier was then used. This oscillator has a frequency accuracy of $\pm$ 0.2% or 0.5 cps whichever is the greater, and an hourly stability of $\pm$0.02%.

The output from the power amplifier was then passed through an impedance matching transformer to give the required oscillation at the rotor conductors. These conductors were connected in series by means of a printed circuit attached to the face of the rotor.

Heavy gauge interconnecting wiring had to be installed as it was found that with light gauge wiring a considerable reduction in output was obtained

over short intervals of time. This was attributed to the fact that the change in resistance of the wiring, due to the heating effect of the load, was greater than the resistance of the conductors.

8.3 Instrumentation

As the amplitudes of the rotor and output oscillations were of a small magnitude, it was essential to have good instrumentation. Barium Titanate strain gauges were tried but it was found that their response was inadequate at the operating torsional frequency of this instrument.

Proximity type gauges coupled to a frequency modulated system were then used. These gauges operate with a 2 megacycle carrier frequency and a maximum modulation of 2%. The sensing unit can be either of the inductance type for moderately large movements, or capacitance type where high sensitivity has to be achieved to measure very small oscillations.

An advantage of this system is that it can be statically calibrated and it gives a sinusoidal output which can be displayed on an oscilloscope.

An inductance type pick-up was used to measure the rotor amplitude and a capacitance sensing unit was made with an effective area of

one square inch and situated parallel to the oscillating gimbal to give an output of 600 mV per thou. displacement (figure 29). The output from these pick-ups, after passing through the frequency modulated system, was either displayed on a cathode ray oscilloscope or valve voltmeter.

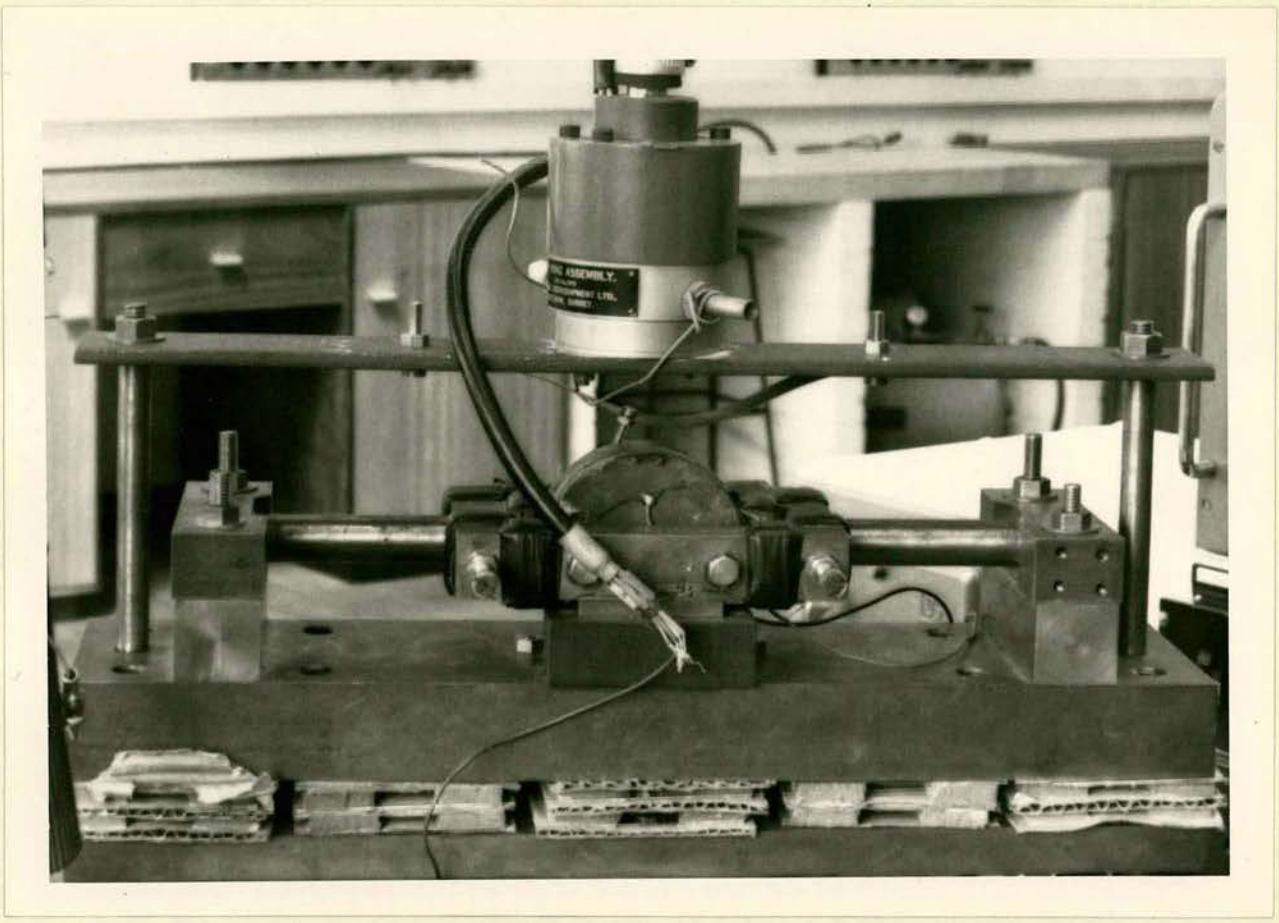

FIG. 29. ASSEMBLED INSTRUMENT ON RUBBER MOUNTINGS.

CHAPTER 9

9.0 Experimental Work

The instrument was assembled and tests carried out at various rotor amplitudes. The variation in amplitude being achieved by altering either the D.C. or A.C. signal to the instrument. Most of the experimental work was carried out with a rotor amplitude, measured at the rotor periphery, of 5.6×10^{-4} ins. It was found that at this amplitude, a reasonable amount of stability could be obtained. At higher amplitudes the system became unreliable due to the heating effect of the increased load.

Graphs of output against applied rate of turn are drawn for each of the varying parameters, axis tilt, mass unbalance, and tilt of the rotor conductors. The theoretical results are drawn lightly and the experimental results superimposed in heavy lines.

The values of output and axis tilt are measured at a radial distance of 1 in.

9.1 Variation in Axis Tilt

Figure (30) shows, graphically, the theoretical and experimental results obtained from the assembled instrument. Initially, it was found that an output signal approximating to a calculated

axis tilt of 0.003 inches was obtained. The instrument was therefore mounted between the centres of a turning lathe and the eccentricity measured and found to be 0.003 inches, thereby substantiating the theoretical curve.

After careful alignment to within an axis tilt of 0.001 inches, the instrument was tested, with varying rates of turn, to give the curve shown on figure(30). This approximated to the theoretical values obtained for an axis tilt of 0.001". During subsequent testing it was found that the bolting arrangement between the inner and outer system yielded to give an axis tilt of approximately 0.002 inches.

9.2 Variation in Mass Unbalance

Figures (31 - 33)show, for various input amplitudes, the signal obtained with an axis tilt of 0.003" and subsequent reduction in this unbalanced effect by adding balancing masses to the periphery of the rotor.

As discussed in Chapter 4.5, a rough balance was carried out with balancing masses added at small angles of β and a large value of the axial displacement 'b'. To obtain more precise balance, masses were then added with β approaching 90° and

the axial displacement reduced slightly.

One of the greatest difficulties in this balancing out procedure was in maintaining the system at its resonant condition. When counter balancing masses were added, the natural frequency of the inner system changed slightly. This reduced the rotor amplitude considerably due to the low damping factors encountered. Tuning of the inner system had then to be carried out after each mass had been added or after its radial distance had been changed.

The outer system had, at each of these balancing procedures, to be retuned by means of the tuning screw to maintain the system as near as possible to its tuned resonant condition.

With large values of axis tilt, e.g. 0.003 ins. the compensating mass required to reduce the unbalanced signal was in the region of 6 gms. This added mass gave an approximate alteration of 1% and 0.1% to the natural frequencies of the inner and outer systems respectively. The balancing masses can therefore be of considerable volume and after fairly short intervals of time they can shift from their positions due to the rotor oscillation. This upsets the balance and tuning of the inner and outer systems with a

consequent reduction in output. However, sufficient results were obtained and figures (31) and (34) show the resulting output when the instrument was balanced out from an initial axis tilt of 0.001 ins. The majority of the experimental work was carried out within the range ±10 Rads/sec. as the variation in output due to damping was pronounced over this range.

Figure 34 shows that the instrument is capable of recording smaller rates of turn with carefully controlled manufacture and instrumentation. The instrument showed greater sensitivity than illustrated in figure (34), but the stability could not be maintained for sufficient periods of time to carry out extensive experimental work.

9.3 Unbalance in the Drive System

As discussed in Chapter 4.3, the conductors inserted in the rotor can, if they are not inserted parallel to the rotor axis, create an unbalanced torque about the output axis. The magnitude of the torque can be varied by altering 'a' (figure 11) the distance through which the electro-magnetic drive force acts about the output axis. This was achieved for the purpose of the experimental work by loosening the bolts which fix the inner rotor

system to the gimbal and then moving the position of the rotor relative to the gimbal along the oy axis. Figure (35) shows the results obtained experimentally for this variation. The rotor was displaced upwards and downwards by approximately 0.010 ins., with corresponding changes in the in-phase component of unbalance. The change in the position of minimum output as well as the intersection of the rate of turn/output relationship gives an indication of the alteration in this unbalanced component and substantiates the analysis of Chapter 4.3. Unfortunately in the present system, the rotor could not be deflected far enough to eliminate this error signal.

9.4 Variation in Damping & Rotor Amplitude

The output from a balanced system operating at the resonant condition can, from equation (27), be expressed as:-

$$\theta_o = \frac{\alpha_o C_1 \Omega}{C_x}$$

For any given applied rate of turn, the ratio of the output to rotor amplitude should be constant, if the damping coefficient is constant. However, as can be seen from Chapter 5, the damping of the outer system is proportional to the output amplitude. As the amplitude is increased, the

output/rotor amplitude ratio will therefore decrease. Figure (36) shows the effect of increasing the amplitude of the rotor oscillation. The dotted graph is for a rotor amplitude of 2×10^{-3} ins., and as considerable heating of the gimbal took place, due to the load on the magnetic coils, some of this reduction in output/rotor amplitude ratio must be attributed to this cause. This could explain the reduction in output when the input was increased beyond 8 Rad/sec. With the present instrument this variation in damping and the heating effect makes it impracticable to operate at high rotor amplitudes.

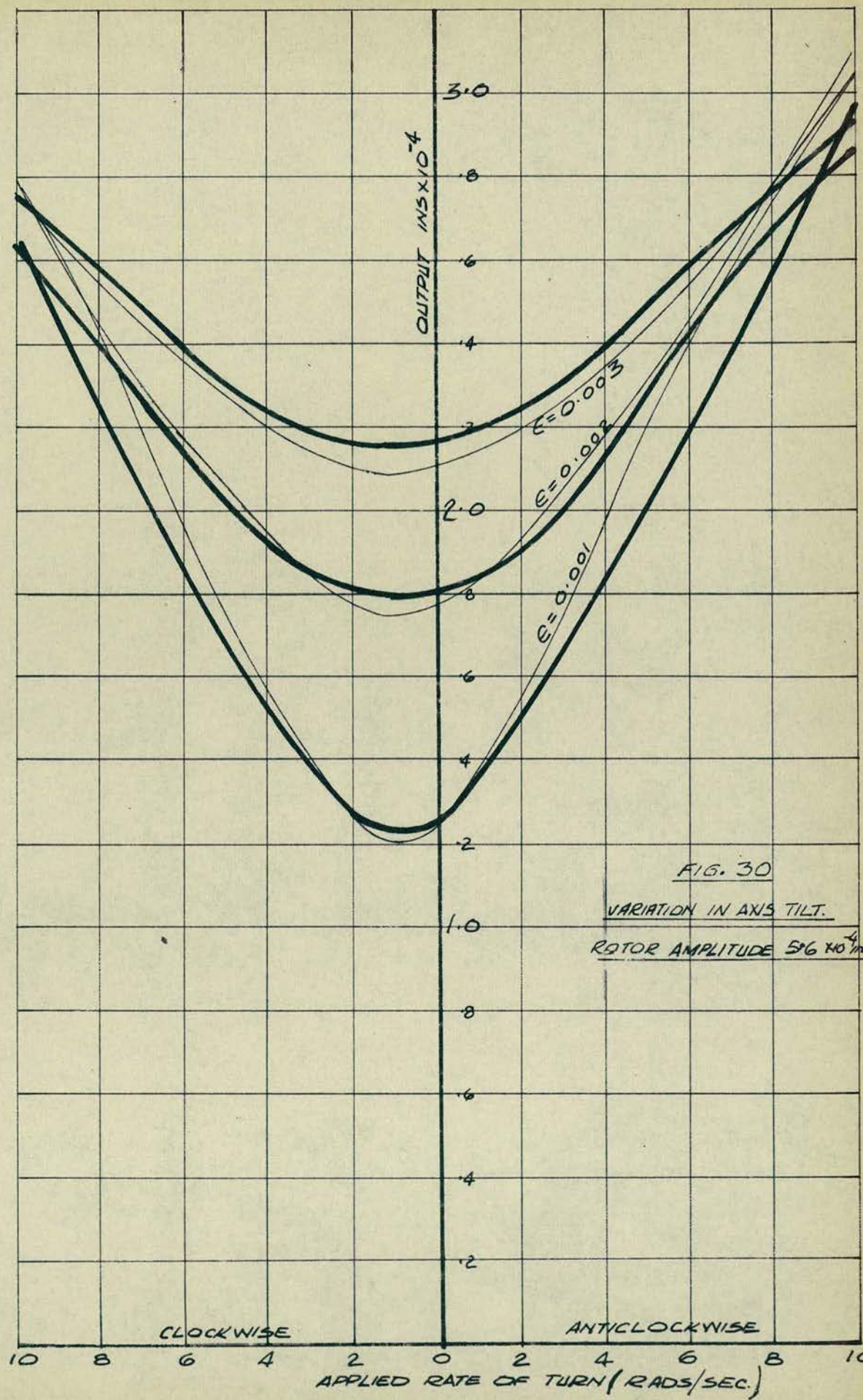

FIG. 30

VARIATION IN AXIS TILT.

ROTOR AMPLITUDE 5.6×10^{-4} INS

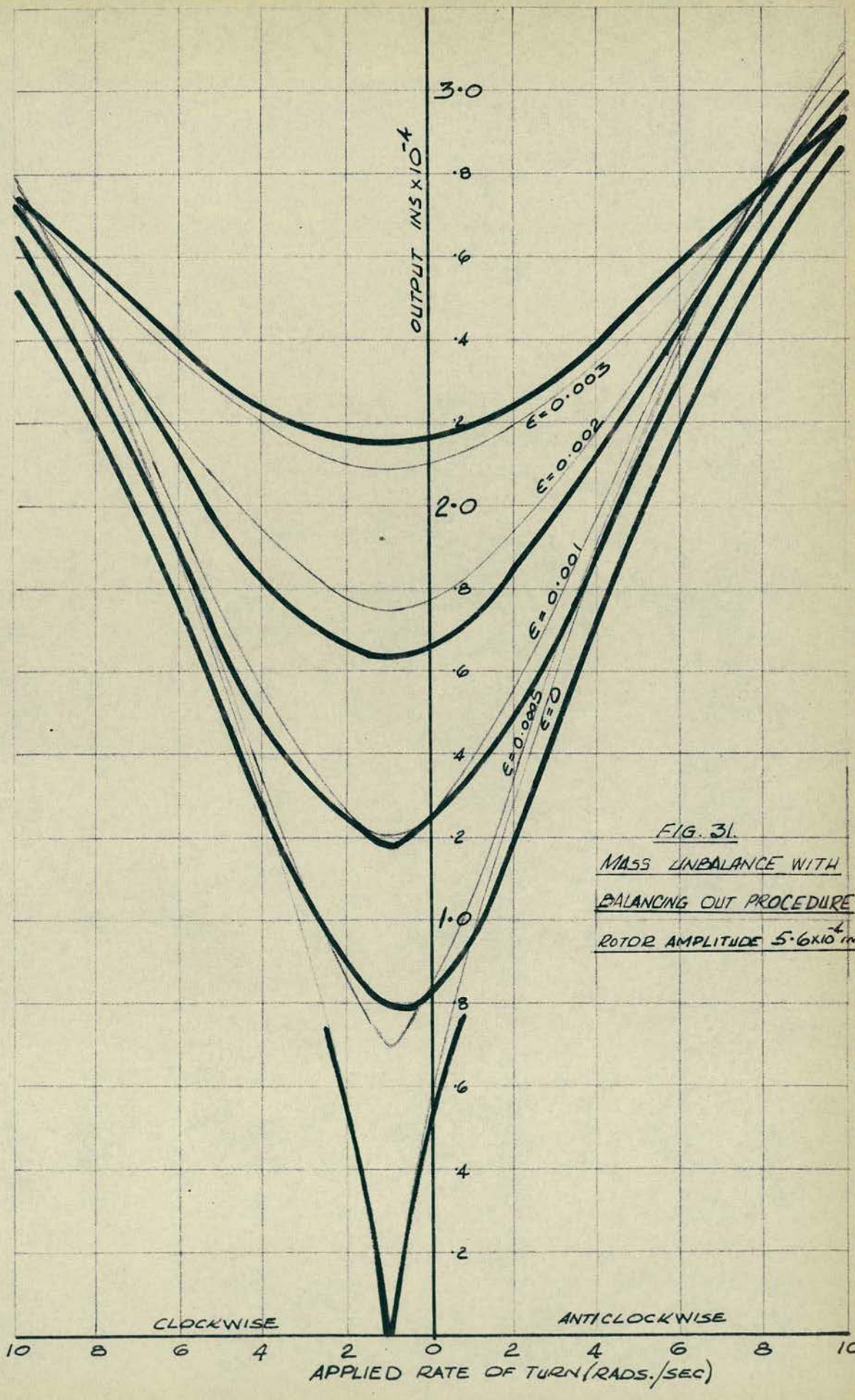

FIG. 31.

MASS UNBALANCE WITH BALANCING OUT PROCEDURE

ROTOR AMPLITUDE $5 \cdot 6 \times 10^{-4}$ INS.

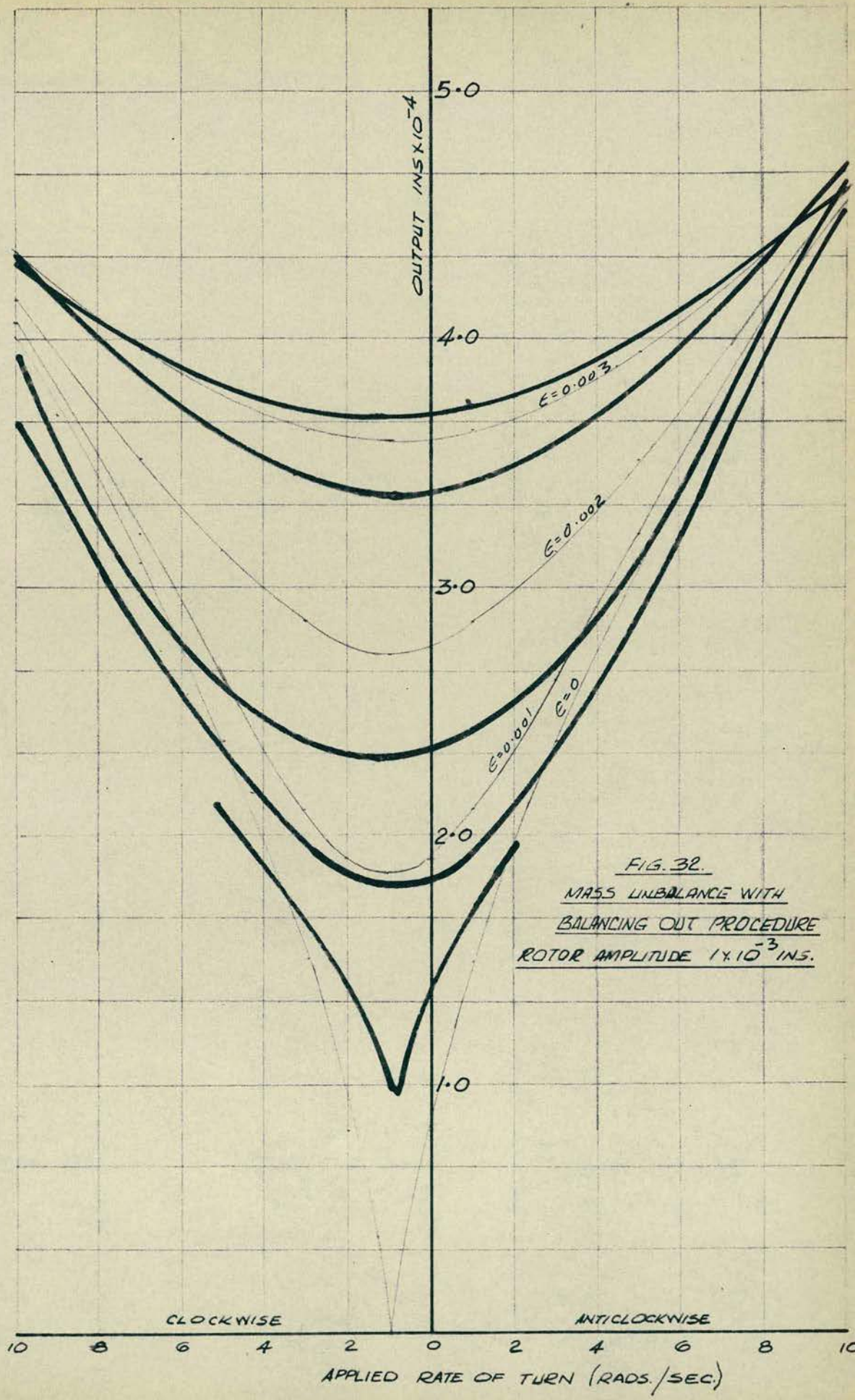

FIG. 32.
MASS UNBALANCE WITH
BALANCING OUT PROCEDURE
ROTOR AMPLITUDE 1×10^{-3} INS.

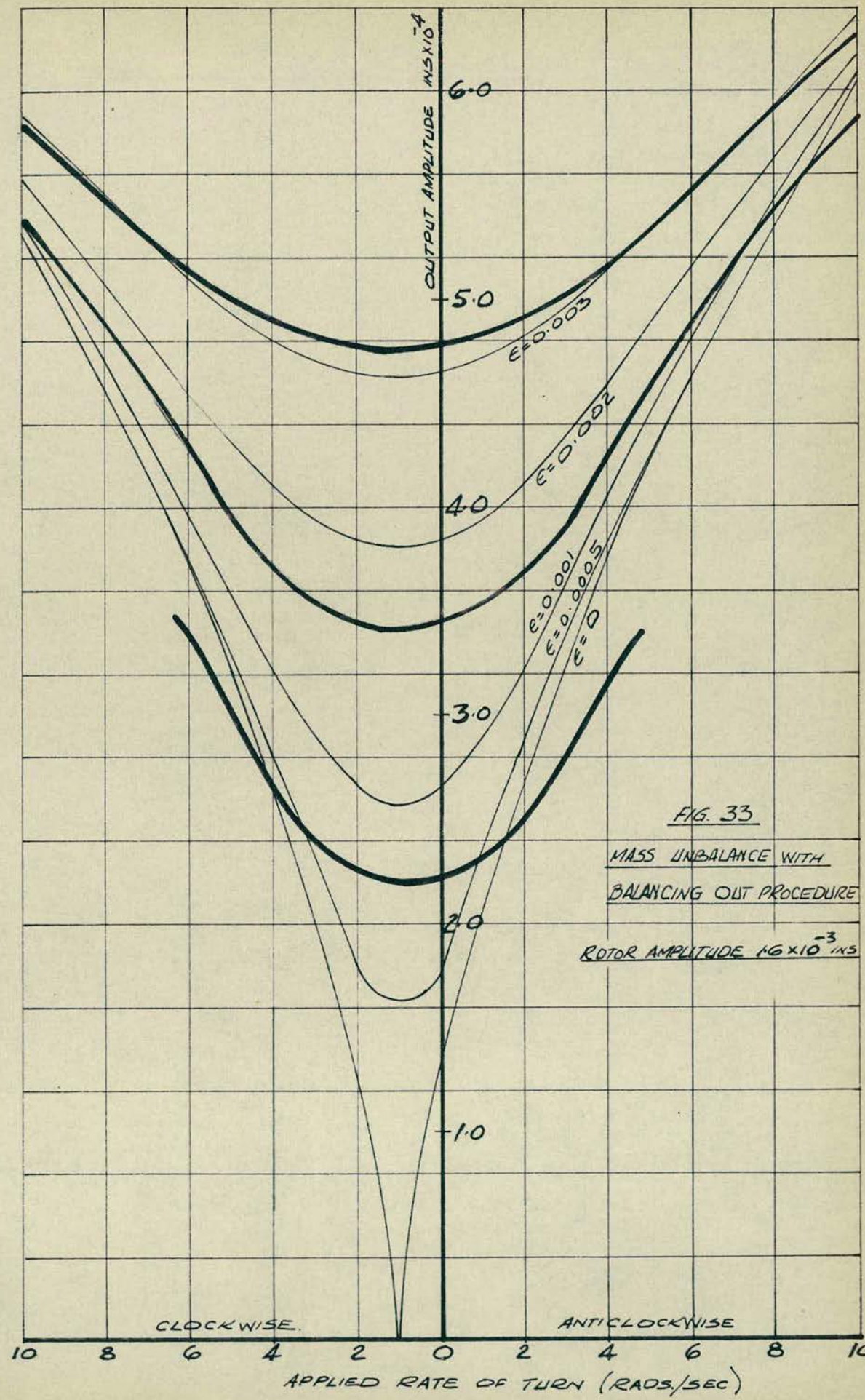

FIG. 33

MASS UNBALANCE WITH BALANCING OUT PROCEDURE

ROTOR AMPLITUDE $\Delta G \times 10^{-3}$ INS

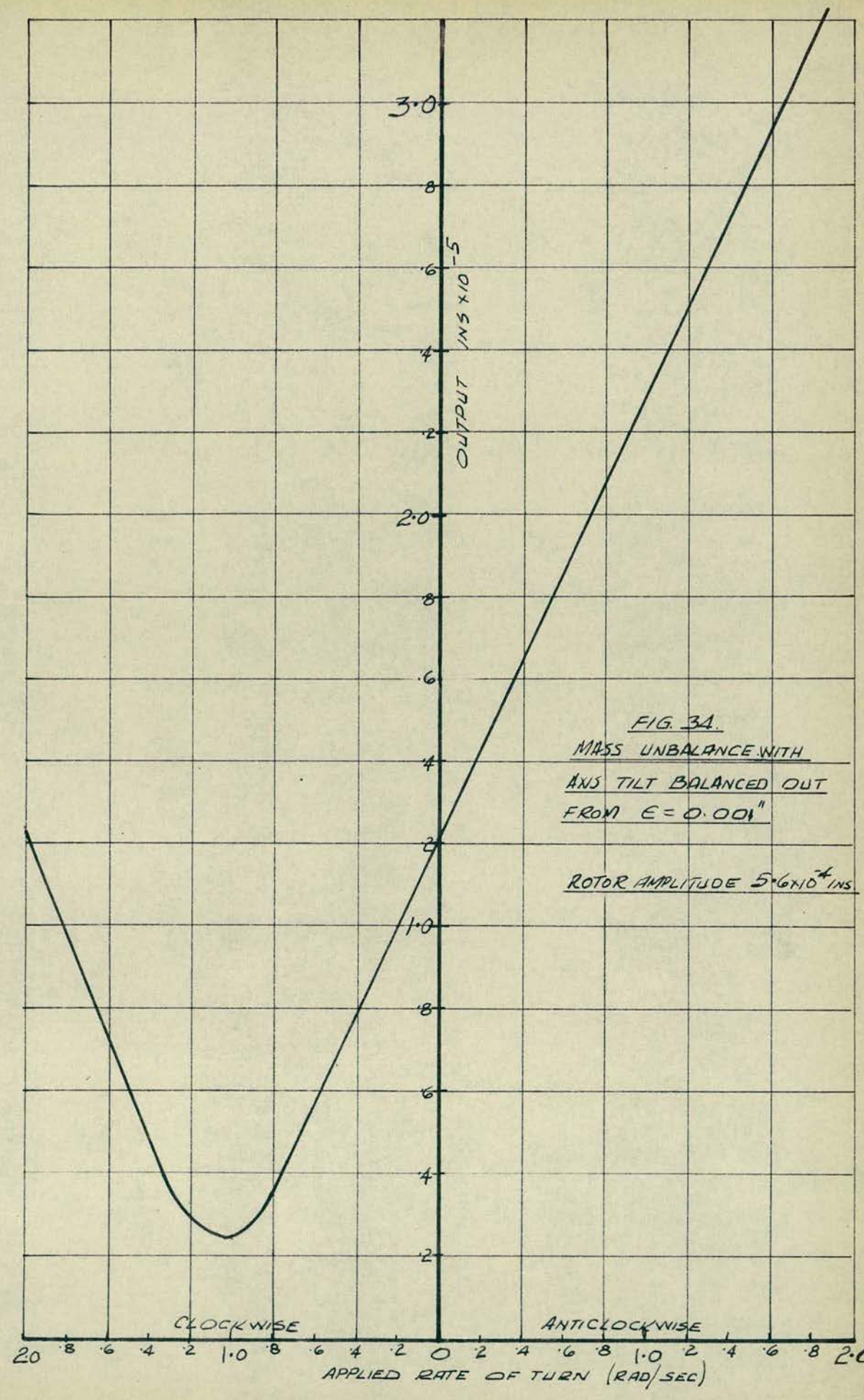

FIG. 34.
MASS UNBALANCE WITH
AXIS TILT BALANCED OUT
FROM $\epsilon = 0.001''$

ROTOR AMPLITUDE 5.6×10^{-4} INS.

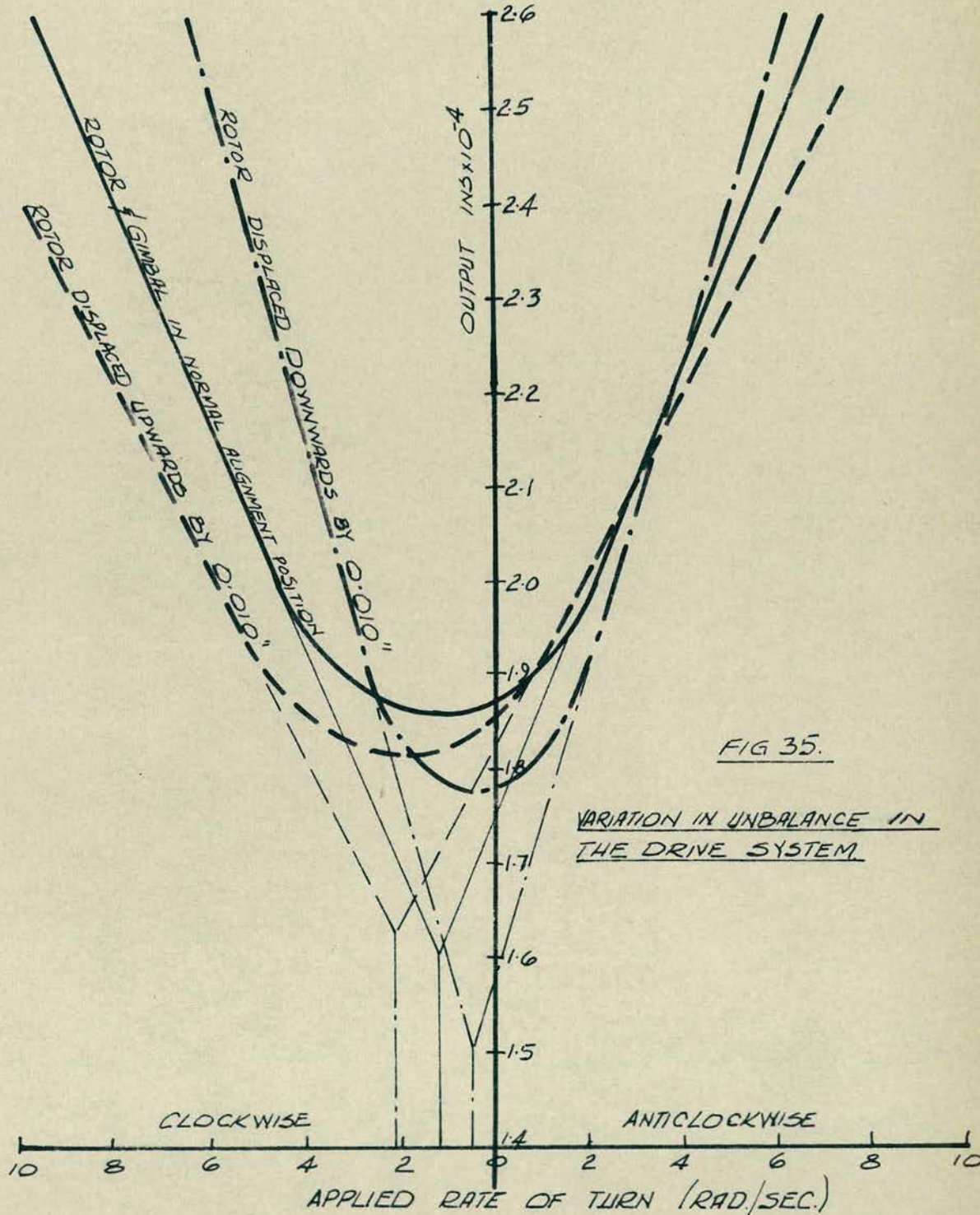

FIG 35.

VARIATION IN UNBALANCE IN THE DRIVE SYSTEM.

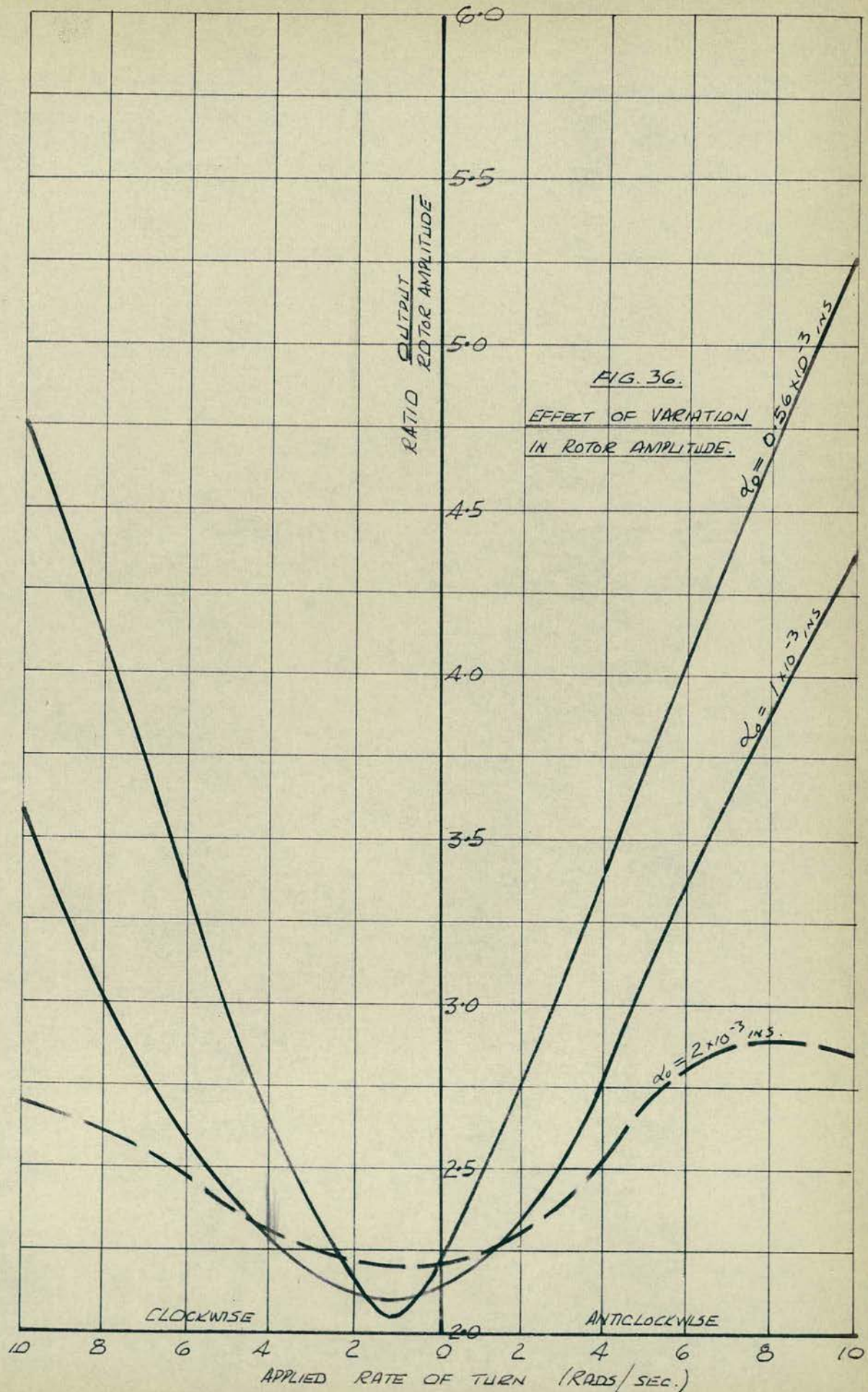
6·0
5·5
5·0
4·5
4·0
3·5
3·0
2·5
2·0
RATIO OUTPUT / ROTOR AMPLITUDE
FIG. 36.
EFFECT OF VARIATION IN ROTOR AMPLITUDE.
$\alpha_0 = 0.56 \times 10^{-3}$ INS
$\alpha_0 = 1 \times 10^{-3}$ INS
$\alpha_0 = 2 \times 10^{-3}$ INS.
CLOCKWISE
ANTICLOCKWISE
10 8 6 4 2 0 2 4 6 8 10
APPLIED RATE OF TURN (RADS/SEC.)

CHAPTER 10

10.0 Conclusions

10.1 Observations on the Comparison of Results

It can be seen from Chapter 9, that there is a considerable measure of correlation between experimental and theoretical results. Most of the experimental work was carried out with an exceedingly low rotor amplitude of 5.6×10^{-4} ins. as it was found that stability could best be obtained at this value. When the rotor amplitudes were increased, the instrument became unreliable because of the increased variation in damping and the heating effect of the magnetizing coils. These factors made it impossible to utilize the high angular momentum anticipated in the design stages. However, it is felt that both of these factors can be corrected in future instruments.

Figure 34 shows that this prototype instrument is capable of recording reasonably small rates of turn, provided the system can be made stable. Some of the instability occurred as a result of the dislodgement of the counter balancing masses due to the oscillation of the rotor. This could be rectified by attaching small balancing screws to the face of the rotor, which would remain fixed in position, after the balancing procedure had been carried out. This would also reduce the other main

cause of instability which occurs due to the requirement that the instrument has at present to be retuned after each subsequent balancing procedure. Adjustment of balancing screws in the direction of the rotor axis would not alter the natural frequency of the rotor system and tuning would then be unnecessary.

In the present instrument the output from the outer system was approximately 600 mV per thou displacement of the gimbal. It should therefore be possible to record changes in input of 0.03 rpm., by using a valve voltmeter having a sensitivity down to 1 mV. A change in output of 0.1 rpm was frequently detected over short periods of time with the present instrument, but unfortunately, the stability could not be maintained over sufficient periods of time to enable results to be repeated and recorded over a range of applied inputs.

It was originally intended to obtain increased stability by operating the instrument at a frequency other than the resonant frequency. However, this was not practicable with the small outputs obtained from this instrument due to the low rotor angular momentum. In the case of the tuning fork, the theoretical results for the effect obtained by tilting the tuning fork in the gravitational field agree very closely with the

experimental results obtained by other authors. This suggests that the explanation for this cyclic variation is, as discussed in Chapter 2.1, due to the axial forces incurred by the effect of the mass of the tines. These forces are tensile or compressive depending upon the position of the tuning fork in the gravitational field, and cause a variation in the potential energy, hence the natural frequency of the tine as it is orientated in the gravitational field.

10.2 Future Design Considerations

Chapter 3.1 shows that the rate of turn signal is proportional to the velocity of the rotor, while the main unbalance effects, which are 90° out of phase with the rate of turn signal, are proportional to the acceleration of the rotor. This suggests that the operating frequency of the instrument should be as low as possible. However, a decrease in frequency has the effect of increasing the time in which the instrument has to be considered inoperative due to the transient response when the input is changed by a step function (Chapter 3.3). The only other way of reducing this transient response is to increase the damping, which is impracticable as it reduces the overall response of the instrument. A convenient means of reducing this transient response must be sought before this instrument can be usefully

employed.

Apart from unbalance, perhaps the main source of uncertainty in this type of instrument is the control or damping. In the present instrument, the damping coefficient was of the order of 0.02 lb.in.sec. and varied proportionally with amplitude. This compared reasonably well with similar tests carried out by Sumner & Entwistle (Reference 7). It was also shown by those authors, and confirmed to some extent by experimentation on the present instrument, that this damping coefficient could be reduced to 0.0005 lb.in.sec. With little variation in the damping over the stress range, this can be achieved by passing a magnetic flux through the rotor shafts and as the damping becomes almost independent of amplitude, a more linear response is obtained from the system. It is therefore suggested that future instruments should have this magnetizing flux flowing through the output shafts. This flux should be independent of the drive system as it has been shown that the increased damping in the inner system of the present instrument can be attributed to electro-magnetic damping. To obtain a greater response from the system this should be avoided.

The present drive system is unsatisfactory and an alternative to this is required. Crystals can be produced with a stability greater than 1 part in 10^9 which suggests that a crystal installed in the rotor or rotor shafts could provide a suitable exciting system for this type of instrument.

10.3 Conclusions

The present prototype instrument behaved basically in the manner predicted. It was limited in these tests to the recording of high rates of turn, principally because of the instability of the instrument at high rotor amplitudes. This was due to the magnitude of the unbalance and the inadequecy of the excitation system. It is shown that these factors can be reduced to enable sufficiently low rates of turn to be detected and thereby justify future work on this type of instrument.

The analysis lays down approximate design graphs and suggests a suitable form of instrumentation. It is anticipated that this type of instrument will have practical applications in the future as there are advantages over the tuning fork which is considered to be a possible replacement of the more conventional type of gyroscope.

It is hoped that the present analysis will assist in predicting some of the characteristics and in the choice of suitable values for the main parameters. of this type of vibratory rate gyro.

REFERENCES

1. Timoshenko, S., - "Vibration Problems in Engineering". (2nd Edition 1937 - Van Nostrand).

2. Den Hartog, J. P., - "Mechanical Vibrations" (4th Edition 1956 - McGraw Hill).

3. Jacobsen & Ayre - "Engineering Vibrations" (1st Edition 1958 - McGraw Hill).

4. Margenau & Murphy - "Mathematics of Physics and Chemistry" (1st Edition 1953 - Van Nostrand).

5. Turnbull, A. W., - "Theory of Equations" (5th Edition 1952 - Oliver and Boyd).

6. Bozorth, R.M., - "Ferromagnetism" (1st Edition 1951 - Van Norstrand).

7. Sumner & Entwistle - "Stress Dependant Damping Capacity" - Journal of the Iron & Steel Institute - Vol. 192 1959.

8. Fopple, O., - "The Practical Importance of the Damping Capacity of Metals Especially Steels" - Journal of the Iron & Steel Institute - No. 2 1936.

9. Pringle, J.W.S., - "The Gyroscopic Mechanisms of the Halteres of the Diptera" - Phil. Trans. Roy. Soc. B, Vol. 233, 1948.

10. Barnaby, Chatterton and Gerring - The Gyrotron Angular Rate Tachometer" Aeronautical Engineering Rev.1953.

11. Lyman, J. - "A New Rate Sensing Instrument" Aeronautical Engineering Rev.1953.